University of Colorado, Boulder
CU Scholar

Undergraduate Honors Theses | Honors Program

Spring 2014

Mineralogy and Genesis of Miarolitic Cavities in Altered Andesitic Dikes on West Spanish Peak, Colorado, USA

Travis Johnson
University of Colorado Boulder

Follow this and additional works at: http://scholar.colorado.edu/honr_theses

Recommended Citation
Johnson, Travis, "Mineralogy and Genesis of Miarolitic Cavities in Altered Andesitic Dikes on West Spanish Peak, Colorado, USA" (2014). *Undergraduate Honors Theses.* Paper 124.

This Thesis is brought to you for free and open access by Honors Program at CU Scholar. It has been accepted for inclusion in Undergraduate Honors Theses by an authorized administrator of CU Scholar. For more information, please contact cuscholaradmin@colorado.edu.

Mineralogy and Genesis of Miarolitic Cavities in Altered Andesitic Dikes on West Spanish Peak, Colorado, USA

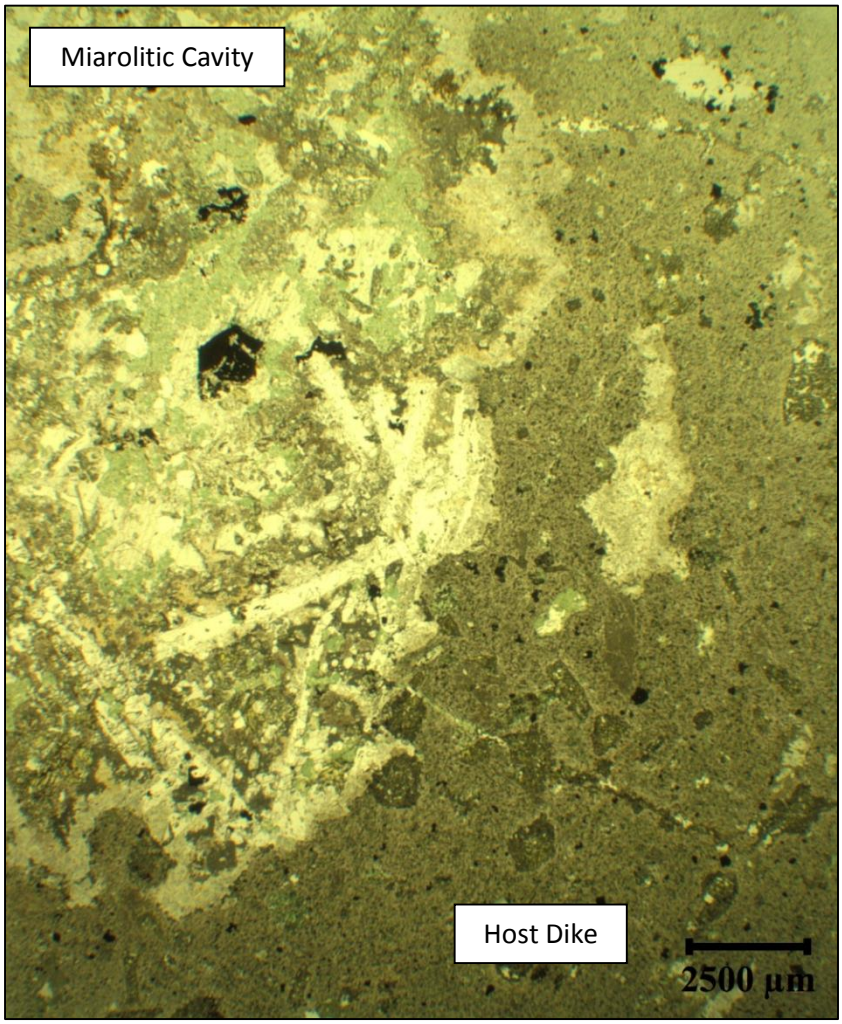

Thesis for Departmental Honors at the University of Colorado Boulder

Travis A. Johnson
Department of Geological Sciences

Defense Date: April 7th, 2014

Defense Committee:

Thesis Advisor: Charles Stern – Department of Geological Sciences
Committee Member: Rebecca Flowers – Department of Geological Sciences
Committee Member: Markus Raschke – Department of Physics

Mineralogy and Genesis of Miarolitic Cavities in Altered Andesitic Dikes on West Spanish Peak, Colorado, USA

Travis A. Johnson
Department of Geological Sciences

ABSTRACT

The focus of this thesis is the mineralogy, chemistry, and the understanding of the origin of small (1-5 cm diameter) miarolitic cavities observed in two altered andesitic dikes on West Spanish Peak, Colorado. Twenty rock samples were collected for analysis, and from them 42 thin sections were made for petrographic investigations. Eight of these thin sections were polished and analyzed with the electron microprobe for chemical compositions of the minerals, as well as identification of opaques. Five samples of cavities and one sample from each host dike were analyzed for trace element abundance using ICP-MS.

The miarolitic cavities taken from West Spanish Peak contain quartz, epidote, chlorite, calcite, muscovite, barite, pyrite, chalcopyrite, hematite, and small traces of a cobalt sulfide. There are some chemical variations within and between epidotes and chlorites, involving inverse correlations of Fe with Al and/or Mg, respectively, as manifested visually by changes in color of these minerals.

The data suggests that Si, Al, Ca, Fe, Mg, S, Cu, Ba, and Co were mobilized within the H_2O, CO_2, and SO_2 bearing fluids that first generated (by exsolution from the magma and expansion) and then mineralized the cavities of both dikes. Potassium mobilization is only observed to occur in one of these dikes, and the absence of any sodium bearing phase in any cavity is noteworthy. Their mineralogy, which is similar to greenschist facies metamorphic assemblages, suggests a process of deuteric alteration occurring within the dikes at >200°C and 500 m depth. The presence of Cu and Co sulfides in these cavities suggests the potential for mineral deposits in the region, consistent with the occurrence of economic metal deposits associated with other Rio Grande Rift related Tertiary plutons to the south of Spanish Peaks.

CONTENTS

Abstract i
Chapter I: Introduction 1
Geological Background 1
Methods 8
Chapter II: Mineralogy 9
Introduction 9
Quartz 9
Epidote 12
Chlorite 14
Calcite 16
Muscovite 17
Barite 18
Opaques 20
Amorphous Mass 23
Chapter III: Mineral Chemistry 24
Introduction 24
Epidote 24
Chlorite 27
Muscovite 30
Chapter IV: Petrochemistry 31
Host Dikes 31
Miarolitic Cavities 33
Chapter V: Discussion and Conclusion 39
Mineralogy and Chemistry of Inclusions 39
Depth and Conditions of Formation 40
Origin of Fluids 40
Implications 41
Future Work 41
Acknowledgements 42
References 43

Chapter I
INTRODUCTION

Geological Background

Miarolitic is a term that has been used to describe cavities observed in igneous rocks that are lined with crystals of various minerals. Miarolitic cavities are typically associated with granitic pegmatites and are formed due to the entrapment of mineral-rich fluids which have segregated by vesiculation of granitic magma during its final stage of crystallization (Kurosawa et al., 2010). Miarolitic cavities typically contain both granitic minerals as well as rare minerals resulting from the concentration of trace-elements by hydrothermal activity and therefore can be a fruitful source for mining operations. Previous studies show that quartz, feldspar, tourmaline, fluorite, and other granitic and hydrothermal minerals are commonly found contained in miarolitic cavities preserved within granites (Candela and Blevin, 1995; Frezzotti, 1992; Kamenetsky et al., 2002; Kile and Eberl, 1999; Kurosawa et al., 2010; London et al., 2012; Peretyazhko, 2010; Pezzotta et al., 1996; Pollard et al., 1991). In all of these previous studies, miarolitic cavities are found near sites of economic significance including large hydrothermal ore deposits, pegmatitic mineral deposits, and gem pockets.

The minerals precipitated into the miarolitic cavities depend on various factors including source rock composition, the amount and composition of volatiles present (carbon dioxide, water, etc.), and the pressure and temperature conditions that the melt solidified under. Petrologic studies of miarolitic cavities can therefore provide geochemical information about the melt from which they were derived and the conditions under which they formed.

The focus of this thesis is the description of the mineralogy and the understanding of the origin of small (<5 cm in diameter) miarolitic cavities observed in altered andesitic dikes on West Spanish Peak, southwestern Colorado (Figure 1.1 and 1.2). The goal of this thesis was to

describe and report the petrological and chemical characteristics of these miarolitic cavities, since no previous studies have reported miarolitic cavities forming within andesitic rocks.

The Spanish Peaks are twin conical peaks (Figure 1.3) located approximately 30 km southwest of Walsenburg and roughly 10 km east of the Sangre de Cristo Mountain range, within San Isabel National Forest in Huerfano Count. East Spanish Peak has an elevation of nearly 12,700 ft (4,200 m) and West Spanish Peak is a little higher having an elevation of about 13,600 ft (4,200 m) (Hutchinson and Vine, 1987).

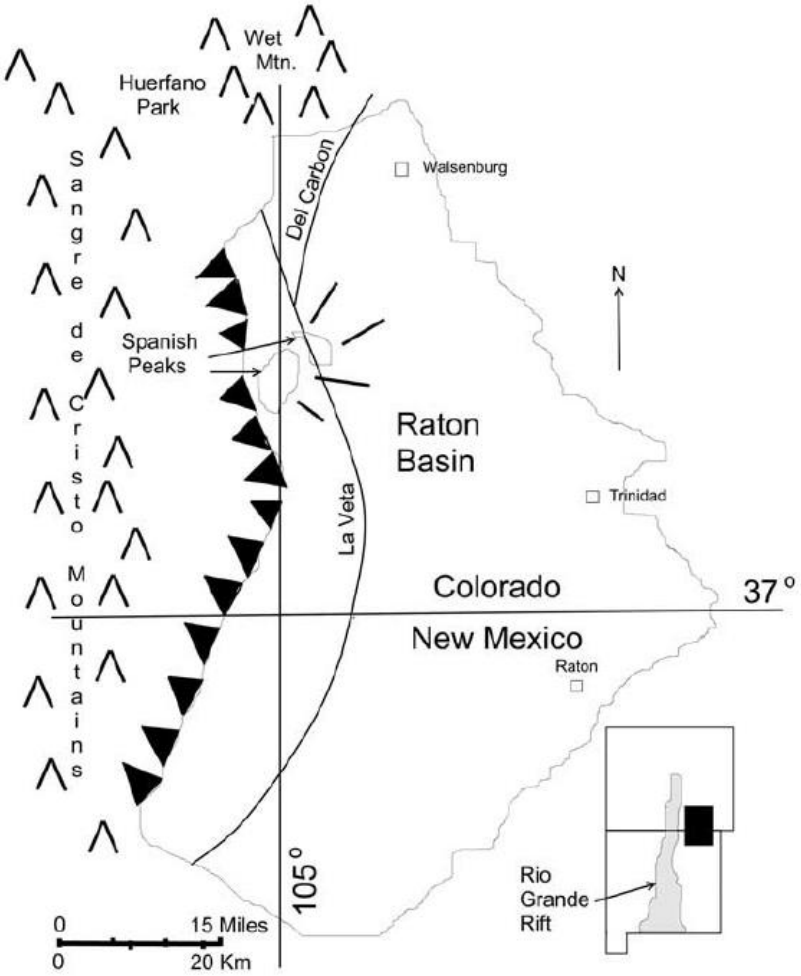

Figure 1.1. Location of the Spanish Peaks along the La Veta syncline within the Raton Basin, in southern Colorado. Adopted from Penn and Lindsey (2009).

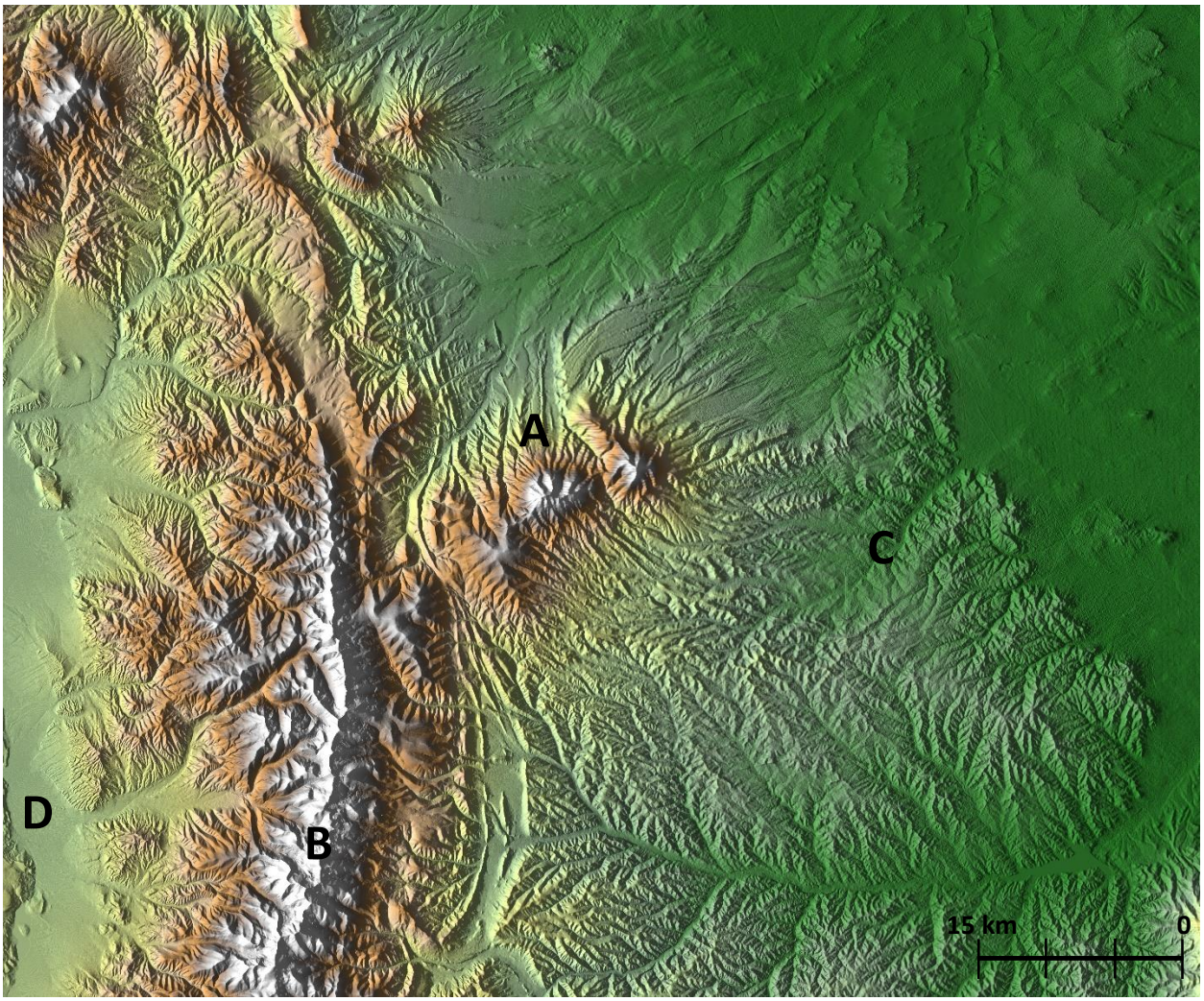

Figure 1.2. Satellite photo image of the Spanish Peak region, just east of the Sangre de Cristo Mountains and the Laramide deformation front in southern Colorado. (A) West Spanish Peak; (B) Sangre de Cristo Mountains; (C) Raton Basin; (D) Rio Grande Rift.

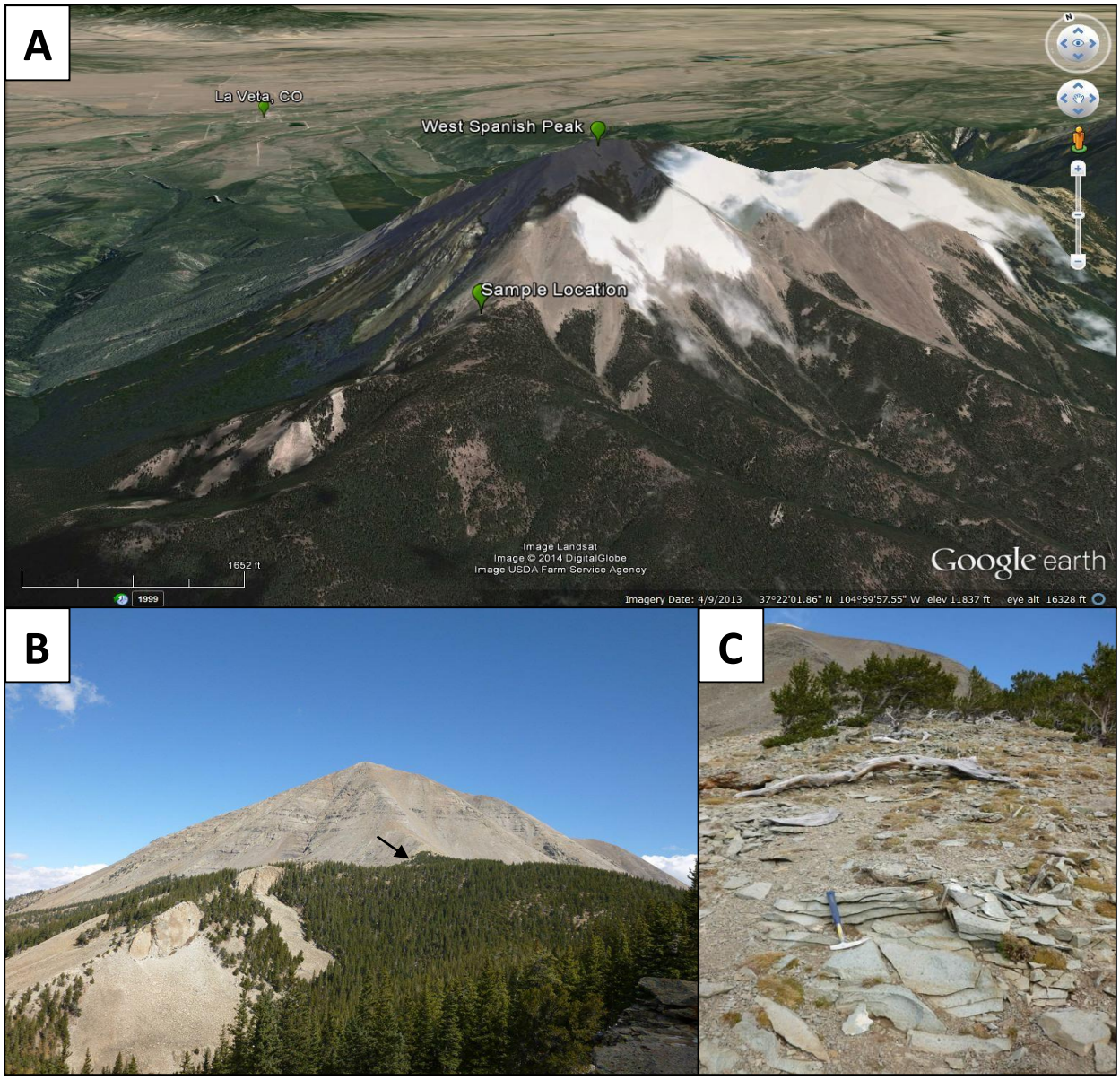

Figure 1.3. (A) Google Earth image of West Spanish Peak, the sample collection location, and La Veta, Colorado, in the background; (B) West Spanish Peak with sample location indicated by the arrow; (C) Close up of the fractured andesitic dike from which samples were collected on the trail up to West Spanish Peak

Spanish Peaks are mid-Tertiary granite/syenite and granodiorite porphyry stocks that intrude Pennsylvanian to Eocene sedimentary rocks (Figure 1.4). They have been dated using K-Ar, $^{40}Ar/^{39}Ar$, and fission track radioactive dating methods (Figure 1.5). The ages determined for East Spanish Peak are ~19.8 - 23.9 Ma. Western Spanish Peak is dated to be ~22.9 - 24.6 Ma (Stormer, 1972; Muller, 1986; Penn and Lindsey, 2009). Based on the age and location of the Spanish Peaks it is commonly accepted that the Spanish Peaks formed during the early phase of extension in the Rio Grande Rift that occurred between ~20 and 30 Ma.

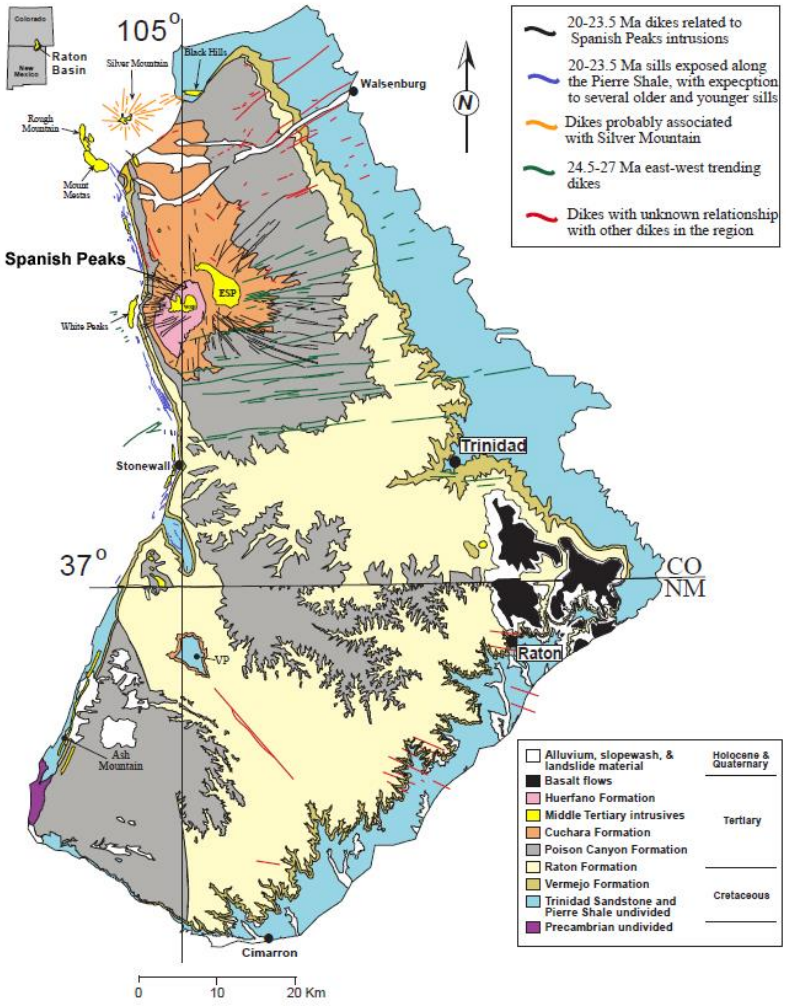

Figure 1.4. Geological Map of the Spanish Peaks area (Miggins, 2002). Radial dikes of the Spanish Peaks are indicated in black.

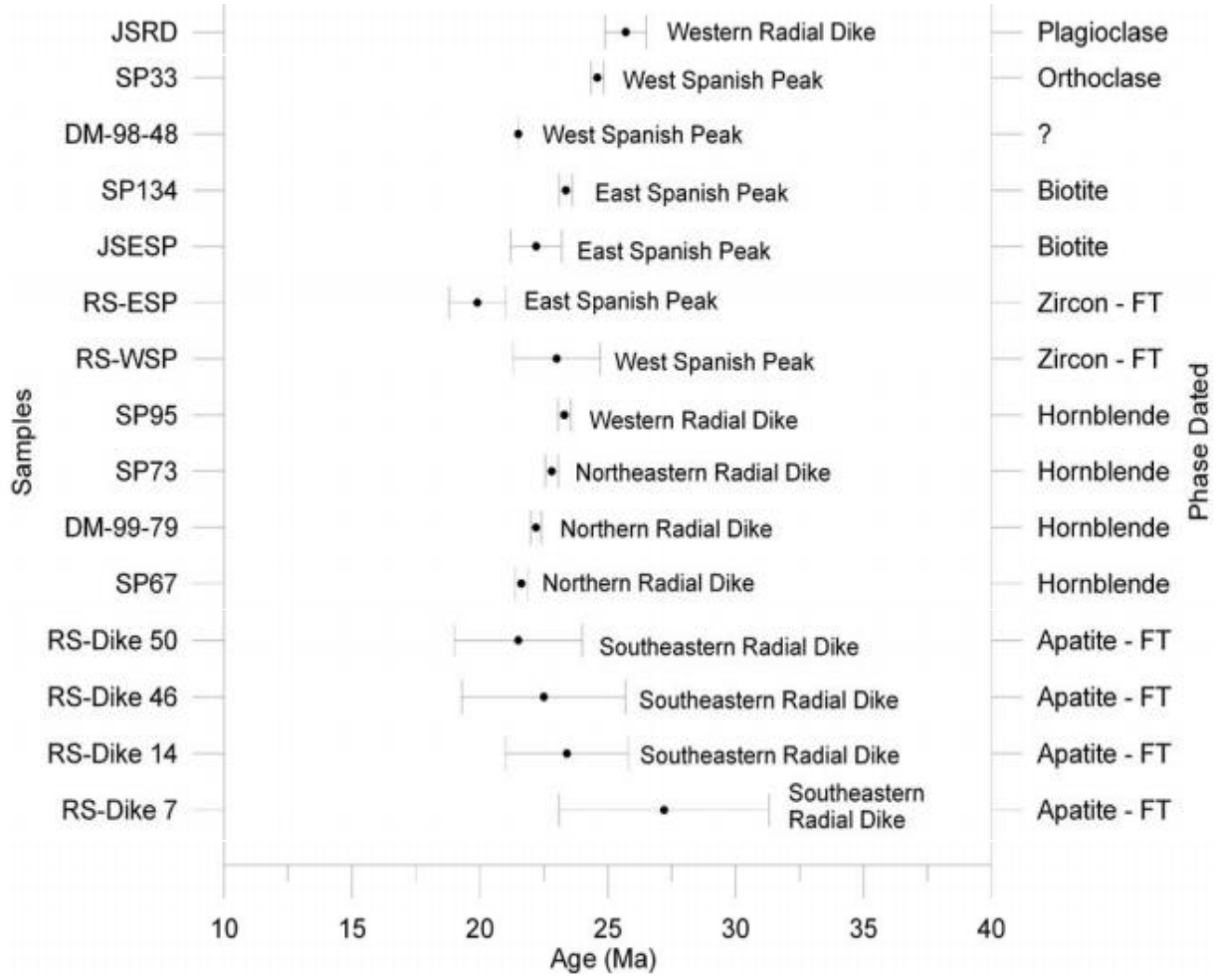

Figure 1.5. Geochronological data for Spanish Peaks stocks and radial dikes; *RS* are from Smith (1975); *DM* are from Miggins (2002); *JS* are from Stormer (1972); *SP* are from Penn and Lindsey (2009). *FT* refers to fission-track technique. Figure modified from Penn and Lindsey (2009).

The Spanish Peaks are noteworthy for a radial dike swarm consisting of hundreds of dikes which surround the two peaks. These dikes are found in greater concentration west of West Spanish Peak. The dikes range from 1 – 100 ft (0.3048 – 30.48 m) in width, stand up to 100 ft (30.48 m) tall relative to surrounding country rocks because they are more resistant to erosion, and are up to 14 miles (22.5308 km) long (Johnson, 1961). These dikes vary in composition and have been identified to be granite, granodiorite, syenite, and syenodiorites.

The miarolitic cavities collected for this study occur in what appears to be two spatially associated altered andesitic dikes that vary slightly in color between a light gray and a slightly darker gray. Besides the small color difference, there appears to be small observable chemical difference between the samples collected, and also a small mineralogical difference in the miarolitic cavities they contain, as will be discussed in more detail in the petrology chapter (Chapter 4), but no contact between these two possibly distinct dikes was observed in the field.

Although hundreds of these dikes surround the Spanish Peaks, it has been suggested that none visibly connect directly with either of the two stocks, nor converge on a single focal point within them. Because of their orientation with respect to the Spanish Peak stocks, it has been theorized that the magmas that formed the dikes may have come from below, and not from within the same magma chamber that crystallized to form the Spanish Peak stocks (Johnson, 1961). Johnson (1961) and Muller (1986) suggest that that these dikes formed the observed radial dike pattern because they intruded into the older joint complex caused by the intrusion of the West Spanish Peak stock.

However, based on my field observations, it appeared as though the dike from which I collected my samples from does merge with the West Spanish Peak stock. Also, new chronologic data suggests potential cogenesis of the radial dikes and the Spanish Peaks stocks (Figure 1.5; Penn and Lindsey, 2009). Although they document an apparent close chronological relationship between the two stocks and nine radial dikes, Penn and Lindsey state that “the complexity of the Spanish Peaks requires more study to ascertain the temporal relationships among the radial dikes” and the stocks. Unfortunately, there is no modern isotopic study that evaluates the potential congenic relationship between the dikes of the radial dike swarm and the Spanish Peak stocks.

Methods

I collected twenty rock samples containing miarolitic cavities from two visually indistinguishable altered andesitic radial dikes near the tree line on the southwest side of Western Spanish Peak (Figure 1.3). Out of these 20 samples, I prepared 42 thin sections using standard thin section making processes, with the additional step of filling in the open spaces with the cavities with hot epoxy cement to make sure that the minerals they contain were not plucked out during the making of the thin sections. From the thin sections I made, 18 were polished for electron microprobe analysis and 24 were covered with petrologic cover glass for examination with a petrologic microscope. Eight of the polished thin sections were selected for electron microprobe analysis to determine chemistry of the minerals in the cavities. The total mineral fillings in five cavities and one sample from each host dike were extracted using a rock saw, powdered and dissolved in HF for ICP-MS trace element chemical analysis.

Chapter II
MINERALOGY

Introduction

With the petrologic microscope, I was able to identify various minerals within the thin sections of the miarolitic cavities, including quartz, epidote, chlorite, calcite, muscovite, barite and opaques. Identification of opaques was based on Energy Dispersive X-Ray Spectroscopy (EDS) scan results. Opaques include pyrite, chalcopyrite, hematite, and one grain of a cobalt sulfide mineral (either cattierite or linnaeite).

Quartz

Quartz crystals within the miarolitic cavities are typically euhedral in shape. Identification of quartz was made based on its low relief, transparency in plane polarized light, and its low-order birefringence colors. Quartz was also easily distinguished based on its unique undulatory extinction. Quartz occurs in all of the samples and is commonly found around the rims of the cavities growing as elongated crystals growing into the cavities (Figure 2.1), although in some cases it occurs only in the center of the cavities. Quartz along the rims of miarolitic cavities typically grow to up to 500 μm in length. In some instances, quartz contains concentric zones of small, neck-down fluid inclusions from which, in most cases, the vapor has escaped (Figure 2.2 and 2.3). These zoned grains of quartz tend to be larger, with a maximum diameter of approximately 1800 μm. In rare instances, quartz grains (up to ~1250 μm in length) contain needle-like mineral inclusions (Figure 2.4).

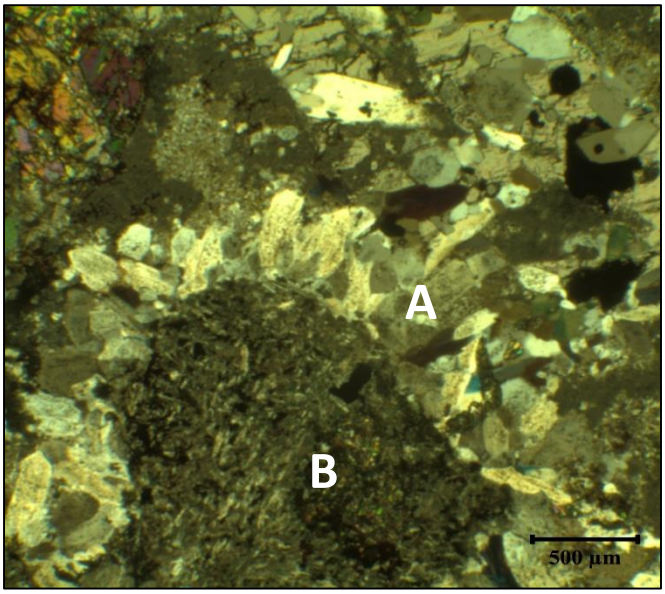

Figure 2.1. Photomicrograph of sample TJ-2A in cross polarized light. (A) Typical elongated euhedral quartz found at the edges of miarolitic cavities. (B) Host andesitic dike.

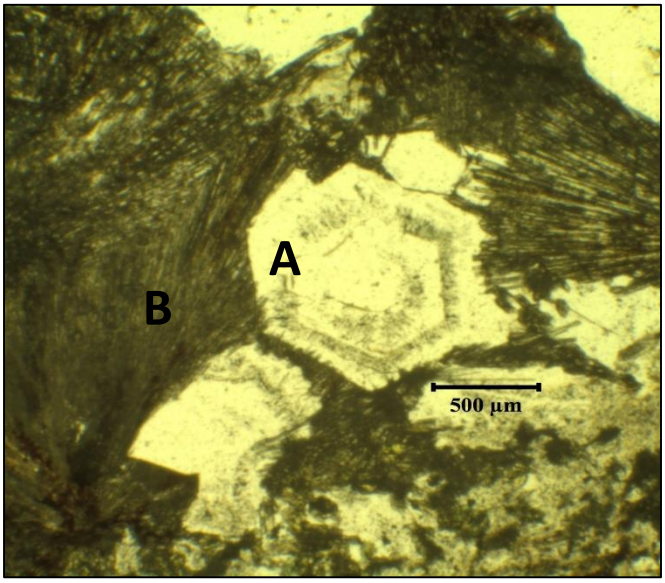

Figure 2.2. Photomicrograph of a section from sample TJ-4A in plane polarized light. (A) Euhedral quartz, approximately 1800 µm in size, concentrically zoned with fluid inclusions. (B) Radial, fibrous epidote grains approximately 2500 µm long from point of growth.

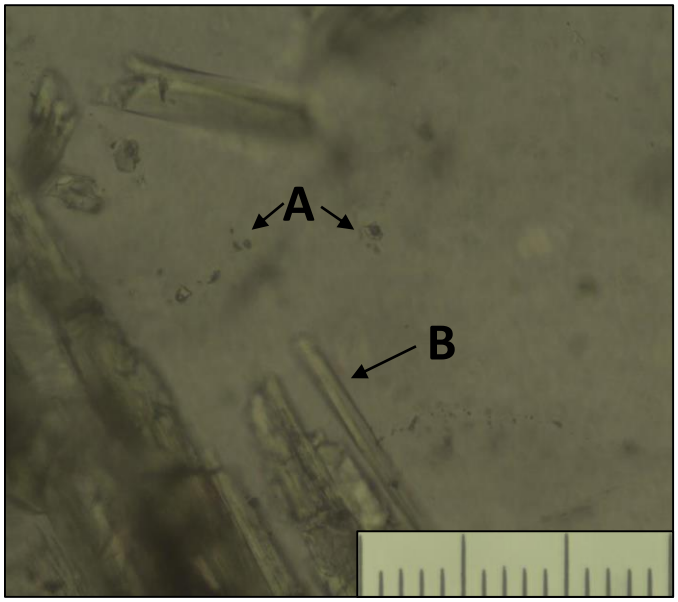

Figure 2.3. Microphotograph of zoned quartz in sample TJ-4A; Each tick on the scale is equivalent to 10 µm. (A) Fluid inclusions typically found in zoned quartz. (B) Small crystals of epidote sometimes found in zoned quartz.

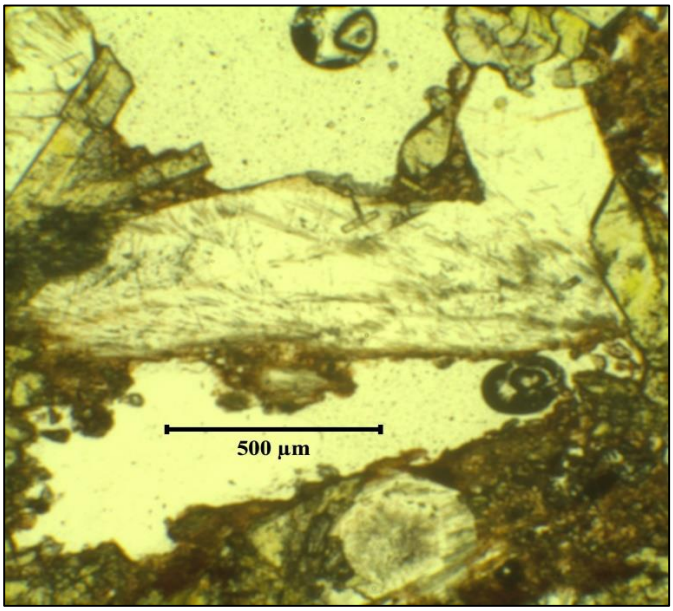

Figure 2.4. Quartz grains from sample TJ-12 filled with needle like mineral inclusions in plane polarized light.

Epidote

Epidote is common in all samples and is commonly found in abundance with quartz. Epidote is distinguished by its yellowish to brownish green color in plane polarized light, its 2-3 order birefringence, and its high relief. Textures observed in my samples include both prismatic (Figure 2.5) and fibrous (Figure 2.2) grains. Fibrous epidote often occurs with quartz crystals containing concentrically zoned fluid inclusions described above. Fibrous epidote can occur with a length of up to ~2500 µm. In some cases, Epidote is chemically zoned, as is easily observable in prismatic Epidote grains due to concentric changes in color and birefringence (Figure 2.6). Epidote tends to vary in location within the miarolitic cavity, but is commonly in a region between the rim and center of the cavity.

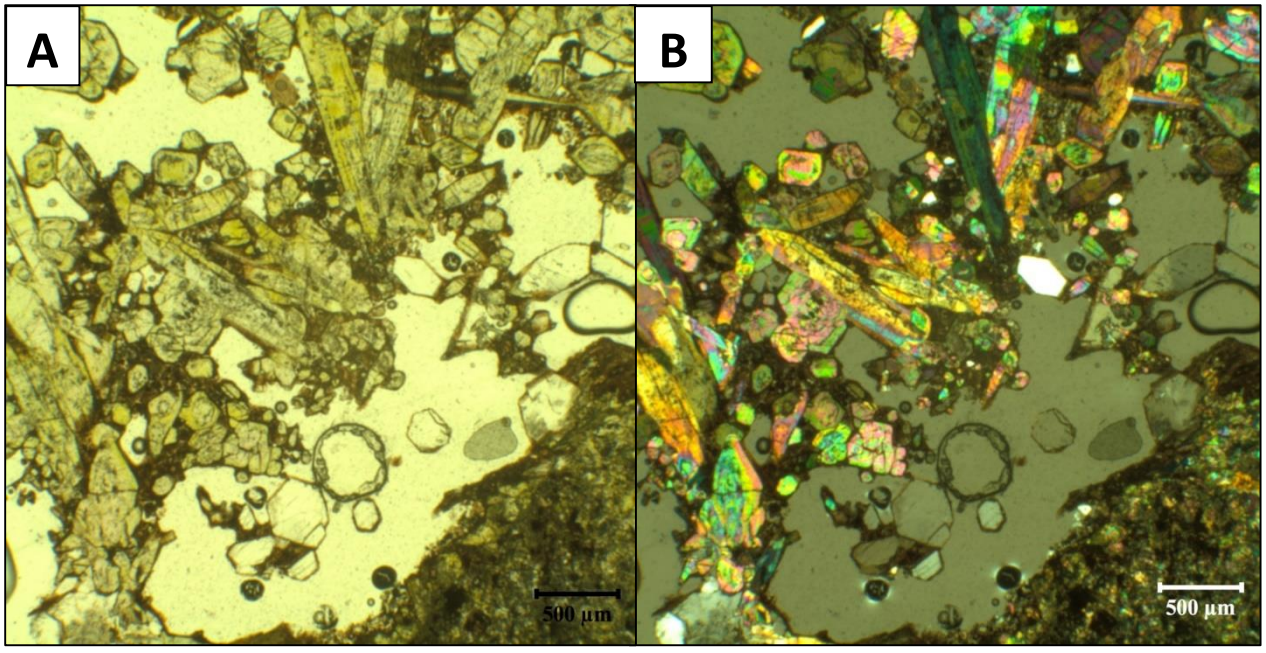

Figure 2.5. (A) Photomicrograph in plane polarized light of prismatic epidote from sample TJ-12 (B) Photomicrograph of prismatic epidote in cross polarized light.

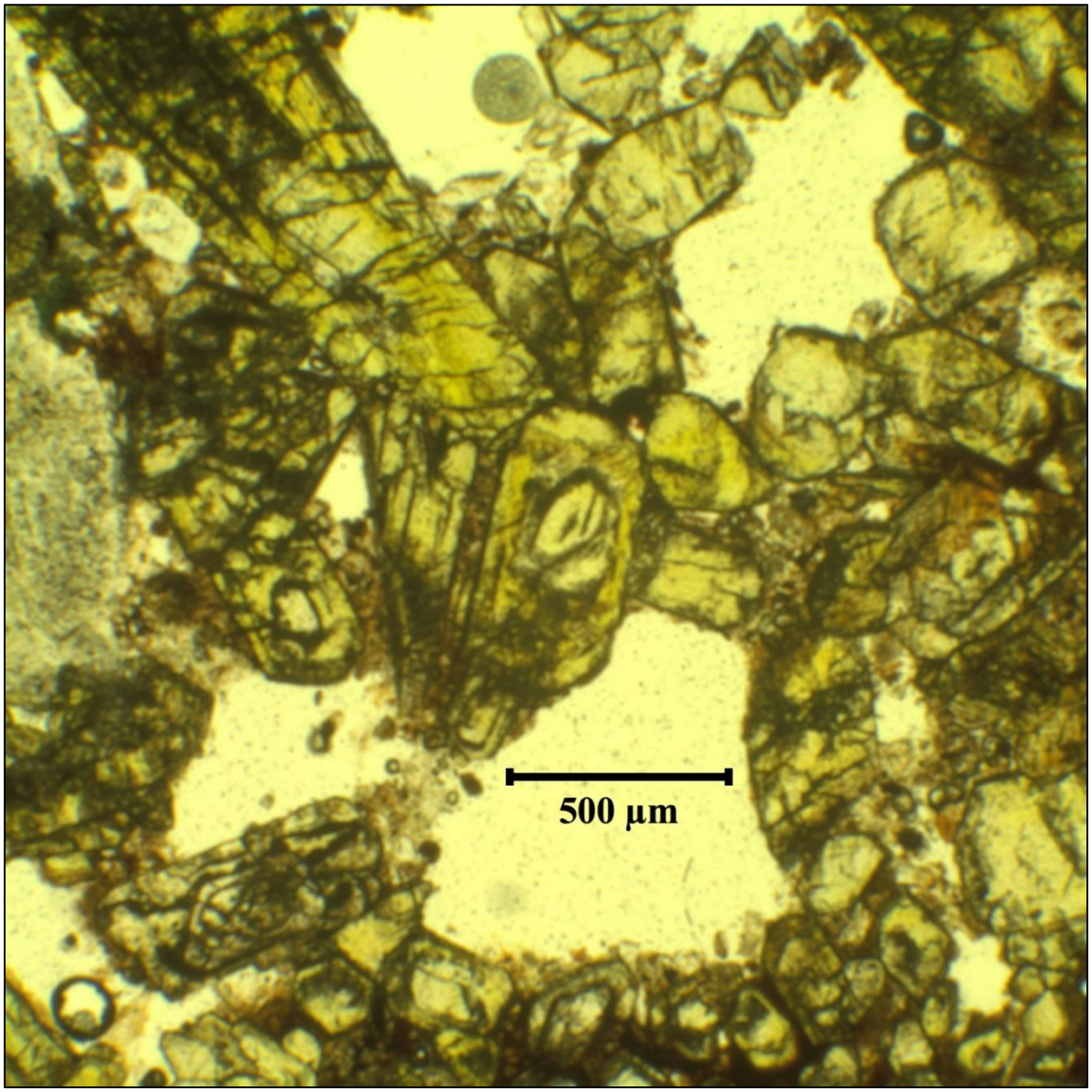

Figure 2.6. Image of zoned epidotes in plane polarized light. The epidote goes from a lighter green center to a darker green rim. The image is from sample TJ-1.

Chlorite

Chlorite is found in many, but not all of my samples. It was identified in thin sections based on its pale to dark green color in plane polarized light and its characteristic anomalous interference colors. In my samples, chlorite is commonly found either in a thin layer at the outer edge of the rim of the cavity (Figure 2.7) as well as within the center of the cavity in larger masses (Figure 2.8). Chlorite also varies in color under plane polarized light from a lighter green (Figure 2.8) to a darker green color (Figure 2.9).

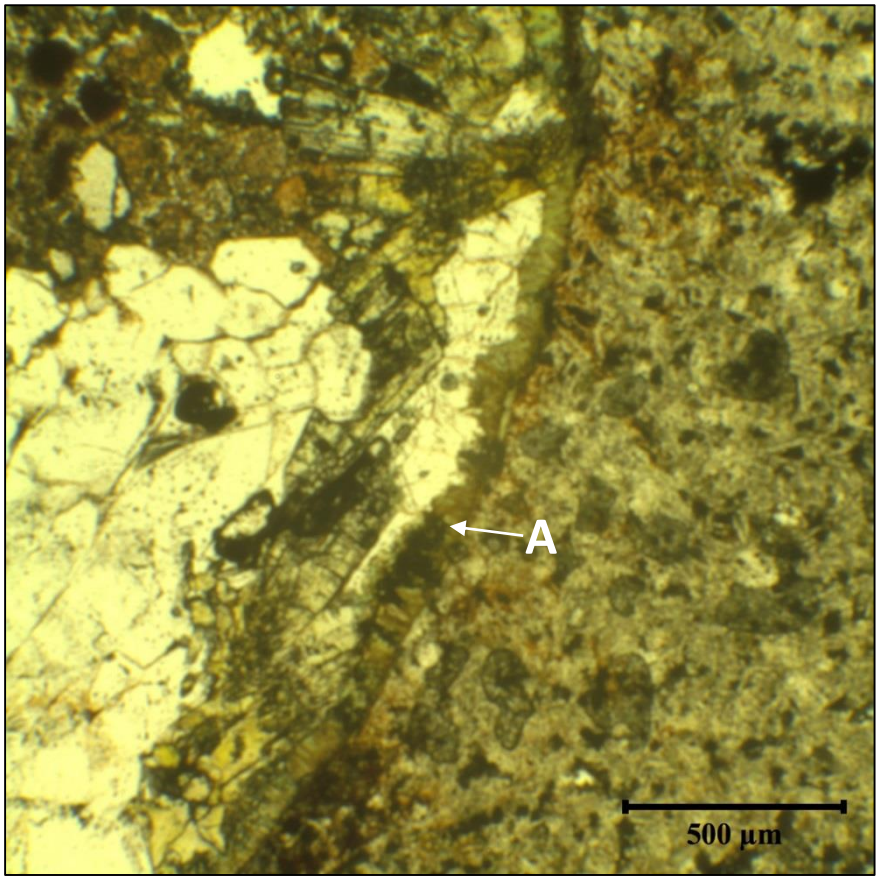

Figure 2.7. Photomicrograph of a miarolitic cavity with a thin chlorite rim (A) in plane polarized light. Image is from sample TJ-5.

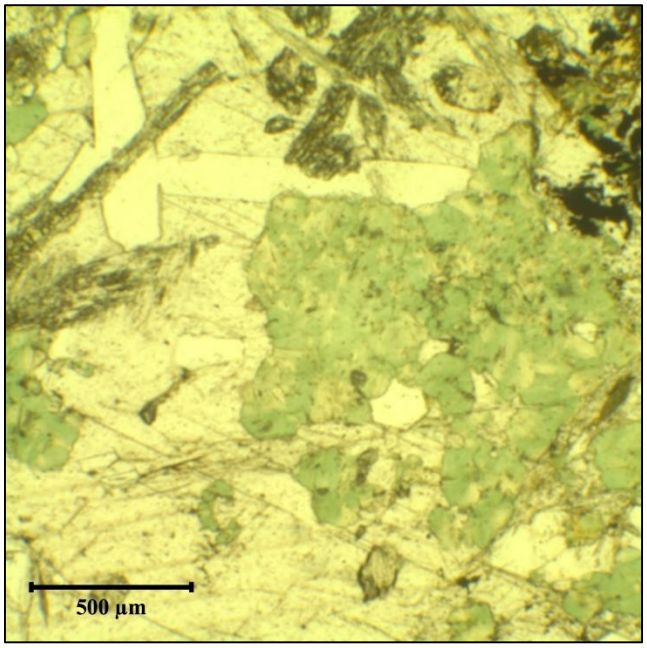

Figure 2.8. Photomicrograph of massive chlorite in plane polarized light. Image is from sample TJ-2A.

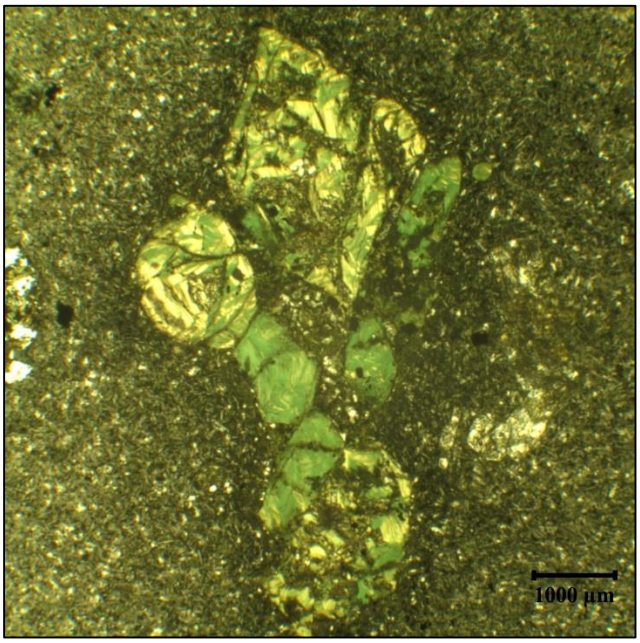

Figure 2.9. Photomicrograph of a miarolitic cavity completely filled with a darker green chlorite in plane polarized light. Image is from sample TJ-4C.

Calcite

Calcite occurs in many of my samples and typically resides in the center of the cavities as large equant or elongated crystals with a maximum size of ~1.1 cm long by 1100 µm wide (Figure 2.10). Calcite was identified under the microscope based on its euhedral shape, high relief, high order white birefringence colors and lamellar twinning. Calcite crystals often contain very clear euhedral quartz crystals (Figure 2.10).

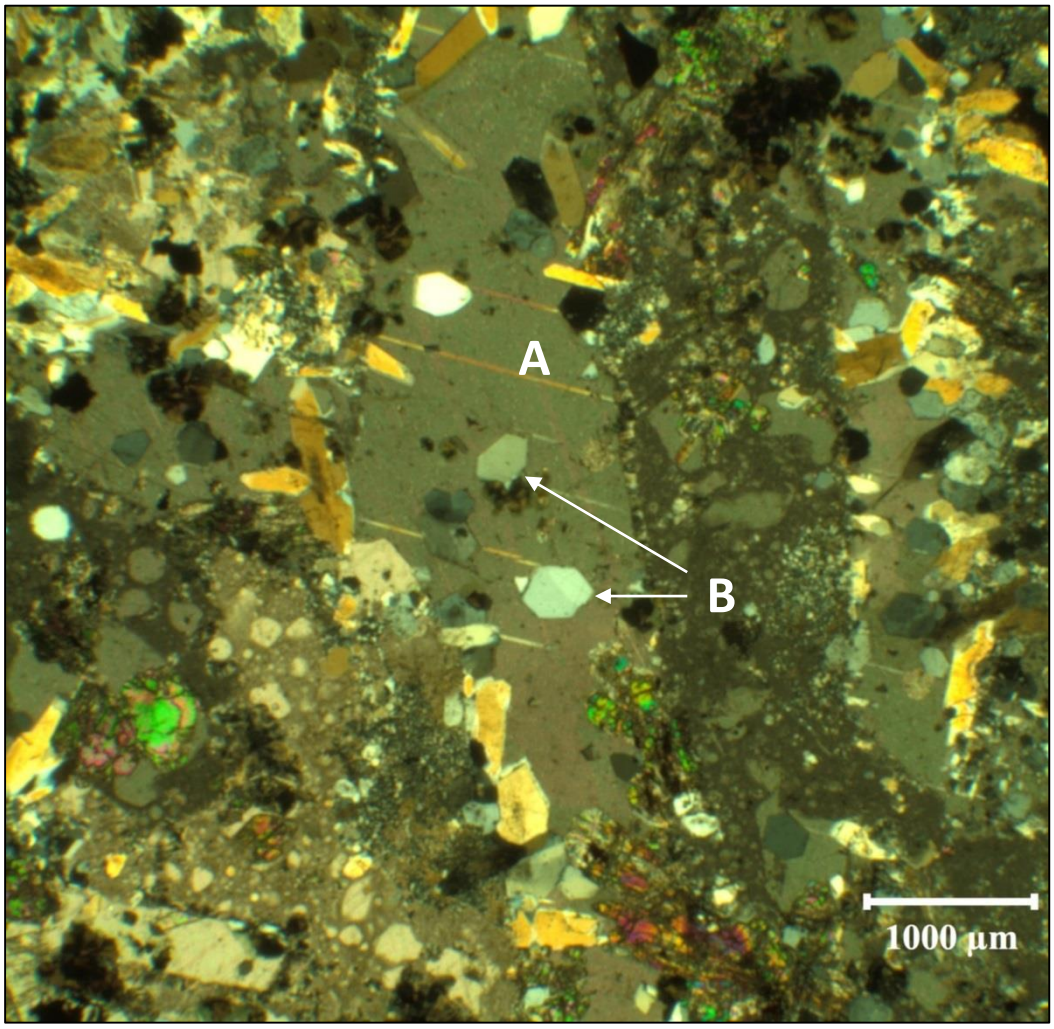

Figure 2.10. Photomicrograph of sample TJ-7E under cross polarized light. (A) Elongated calcite crystal. (B) Small, clear euhedral quartz within larger calcite grain.

Muscovite

Muscovite is found only sparsely in my samples. Muscovite was identified based on it being colorless in plane polarized light, its perfect cleavage, and having high order interference colors with bird's eye texture. In relation to the miarolitic cavity, muscovite is typically observed near the center and is fibrous in shape (Figure 2.11).

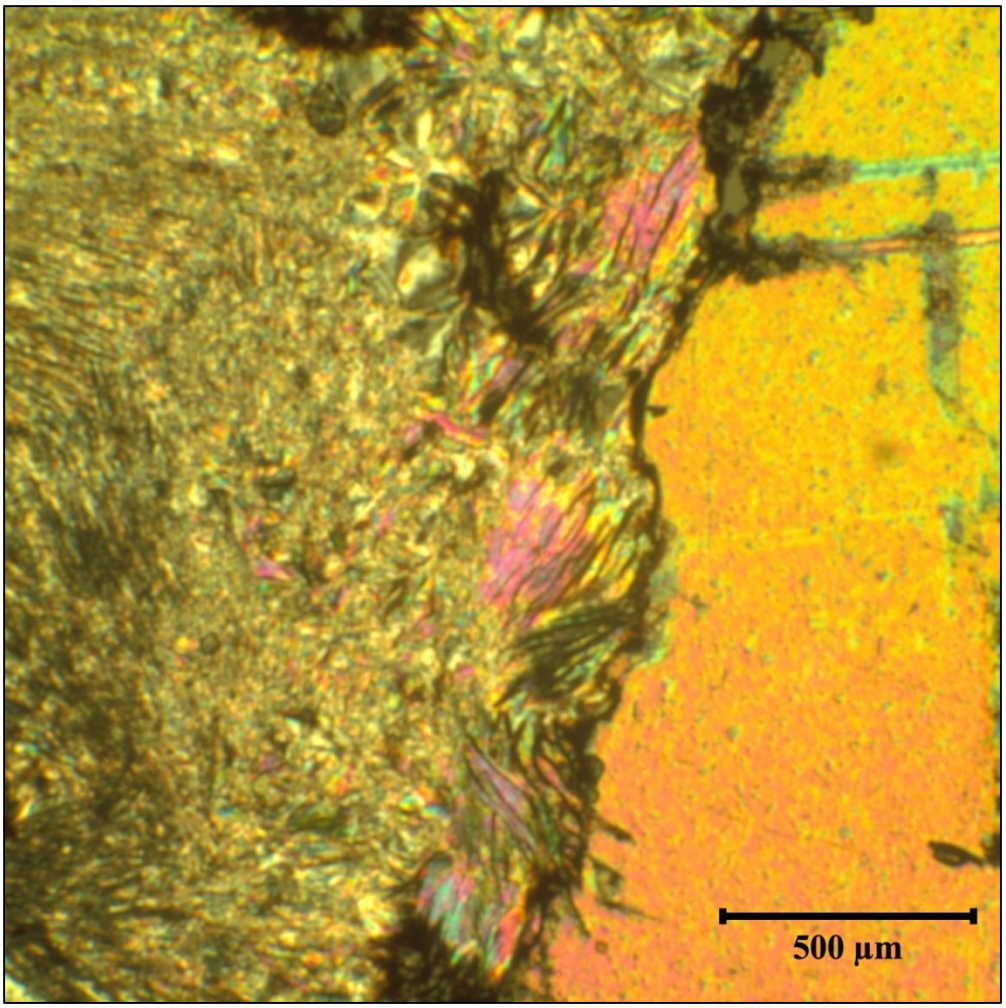

Figure 2.11. Photomicrograph of fibrous muscovite in between a large calcite grain and a fibrous epidote in cross polarized light. Picture is from section of sample TJ-3.

Barite

Barite was not initially identified in the petrologic microscope as it appears throughout the cavities as small, colorless grains (Figure 2.12). Barite was observed and identified initially using the EDS of the electron microprobe (Figure 2.13).

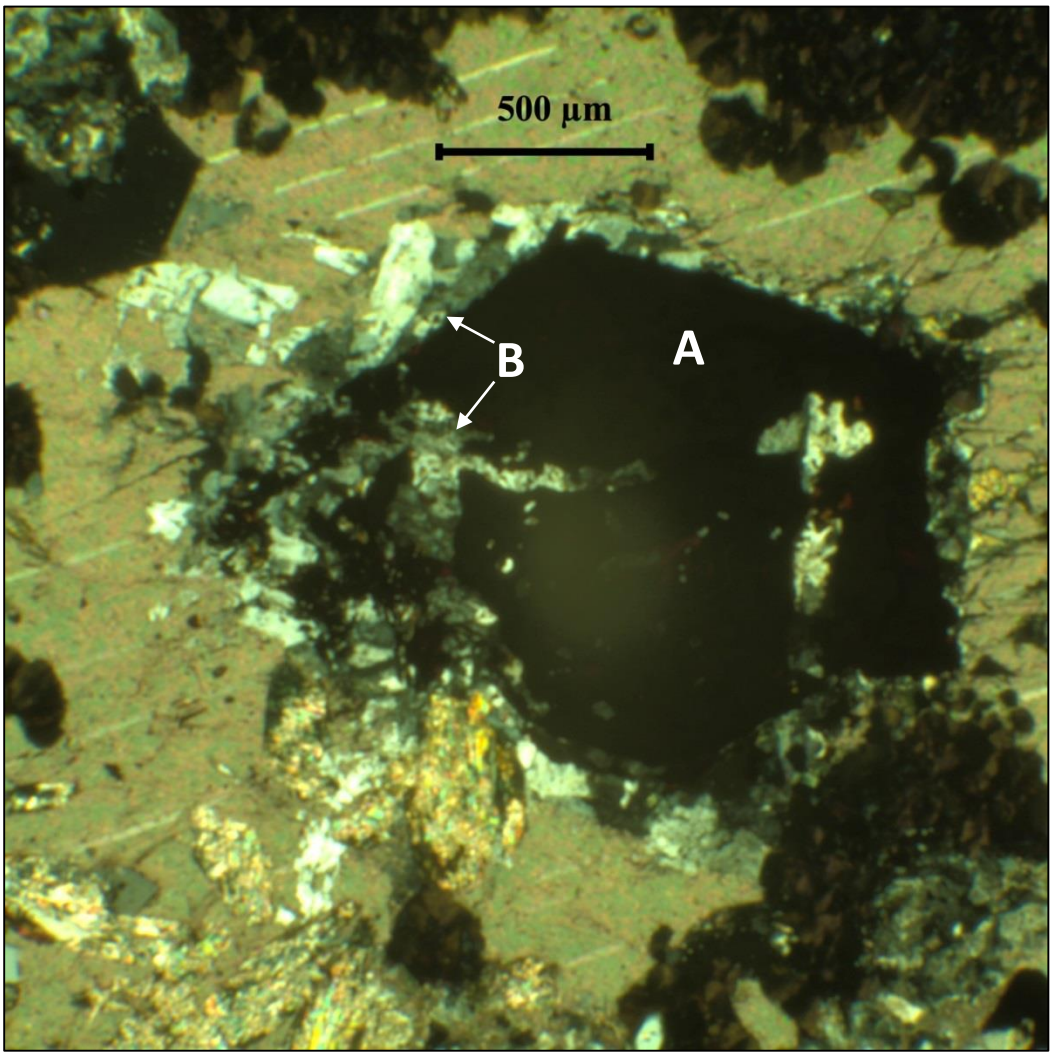

Figure 2.12. Photomicrograph sample TJ-2A in cross polarized light. (A) Large opaque which consists of a chalcopyrite grains surrounded by hematite and (B) Barite surrounding and cross cutting the opaque.

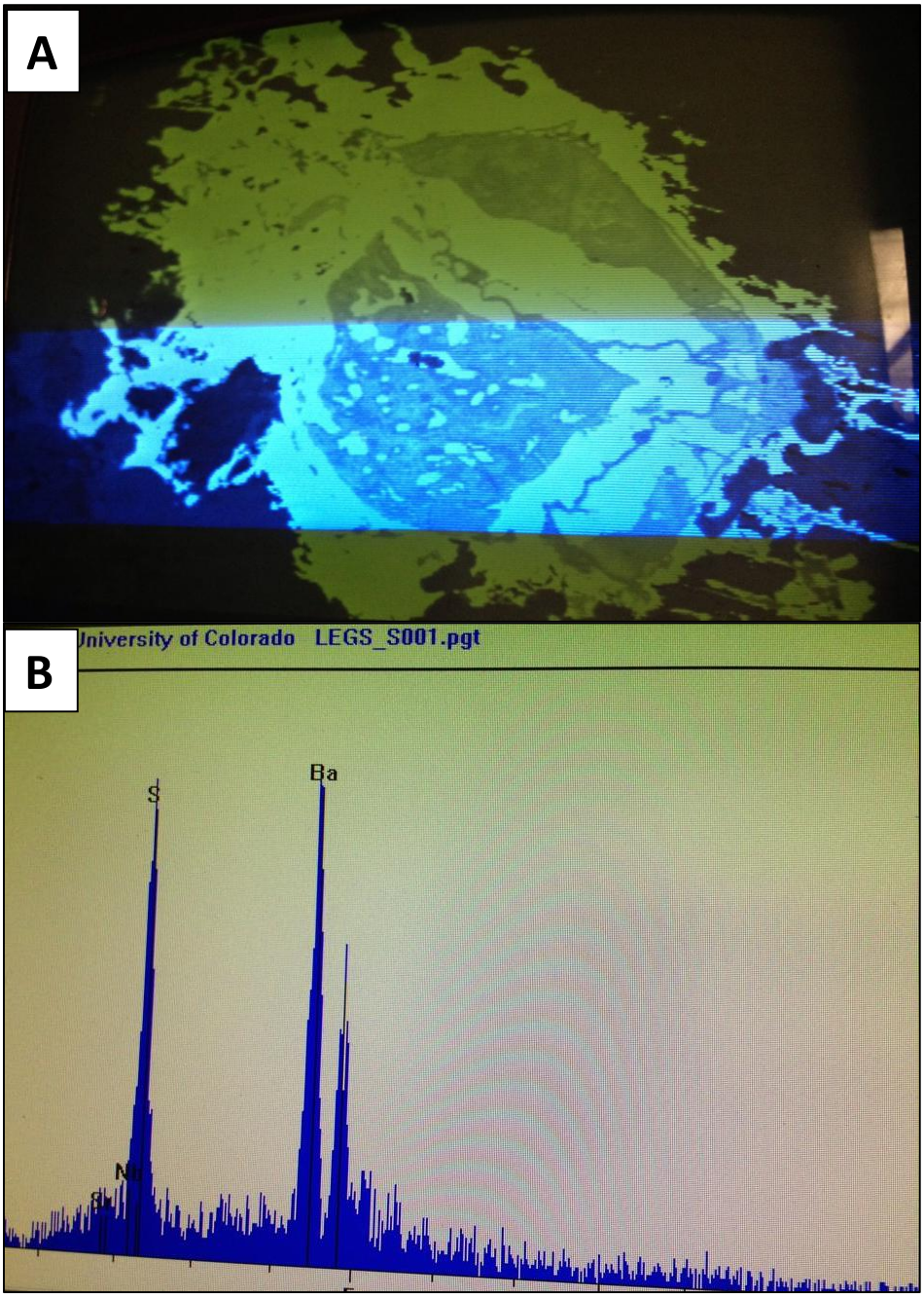

Figure 2.13. (A) Backscattered electron image of large opaque figure 2.12. Barite is the bright white mass that surrounds and cuts through the large opaque. (B) EDS results for the large white mass surrounding the opaque, identifying the mass as Barite. Note scale in Figure 2.12.

Opaques

All observed opaques were identified using EDS of the electron microprobe. The opaques identified include: Pyrite, Chalcopyrite, Hematite, and one small grain of a Cobalt Sulfide mineral (either catterite or linnaeite). Pyrite and Chalcopyrite is ordinarily found with each other near the center of the cavity (Figure 2.14) while hematite are usually scattered within the cavity, either surrounding the sulfides in a botryoidal texture or as independent platy laths (Figure 2.15). One small cobalt sulfide mineral (either catterite or linnaeite) was observed near the center of a larger opaque consisting of chalcopyrite (Figure 2.16). This is the only observed appearance of cobalt sulfide found in all of the samples that were examined with the electron microprobe. Opaques typically are smaller with a maximum diameter of ~1800 µm and are scattered throughout the cavities.

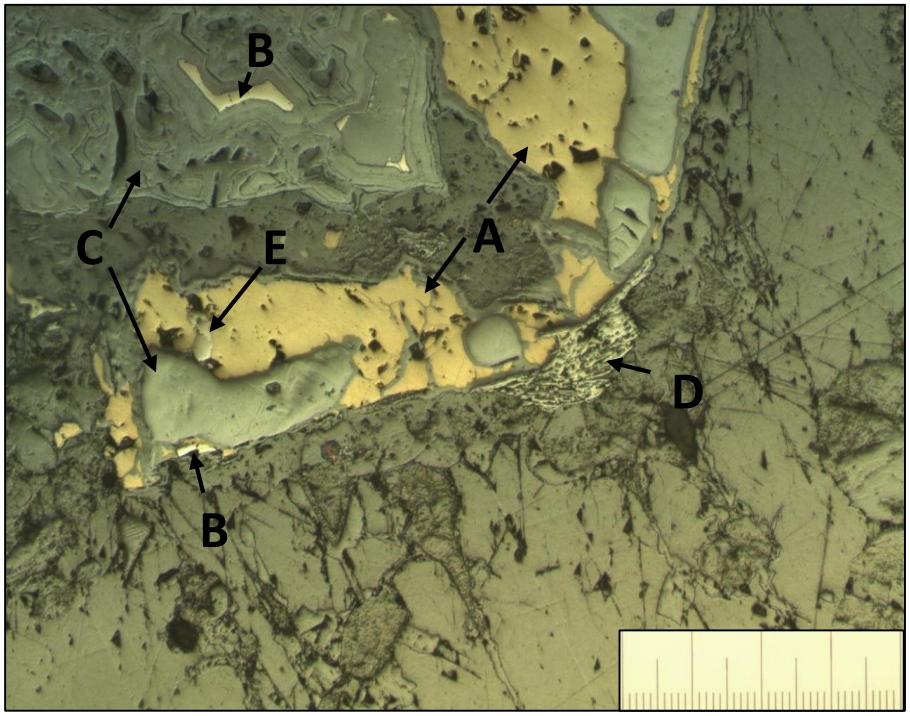

Figure 2.14. Microphotograph of section of large opaque (Fig. 2.12) in sample TJ-2A in reflected light. (A) Chalcopyrite; (B) Pyrite; (C) Botryoidal Hematite; (D) Platy Hematite (E) Cobalt Sulfate. Each large tick on the scale represents 1/10th mm.

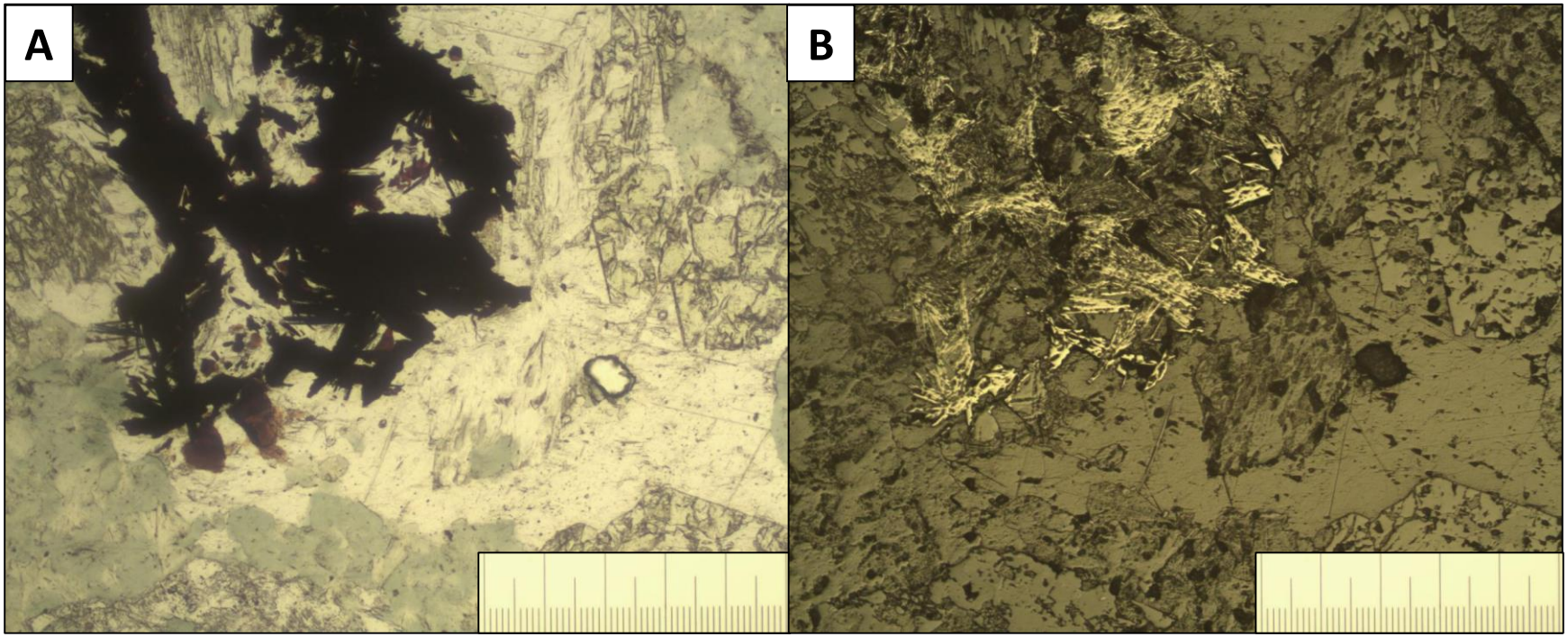

Figure 2.15. Microphotographs of platy hematite from sample TJ-2A in (A) plane polarized light and (B) reflected light. Each large tick on the scale represents 1/10th mm

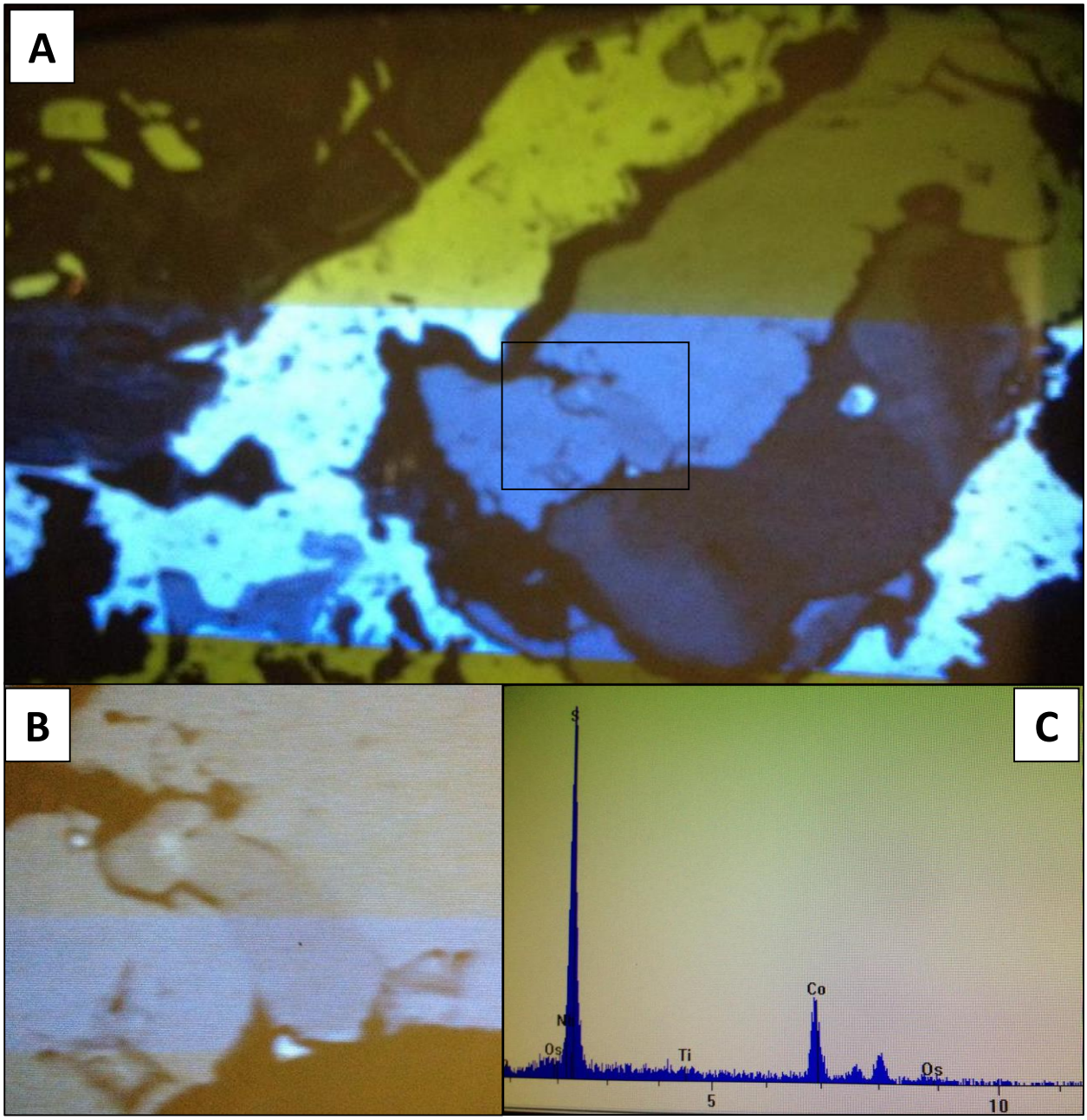

Picture 2.16. (A) Backscattered electron image of area within large opaque. Outlined box contains the identified cobalt sulfide mineral within chalcopyrite. (B) Close up of outlined box in (A) containing the identified cobalt sulfide mineral. (C) EDS results of the darker mineral in (B). Results indicate the mineral is a cobalt sulfide. Note scale in Figure 2.14 for (A) and (B).

Amorphous Mass

Within some of my samples, there are amorphous masses that are unidentifiable. They appear to be brecciated material containing broken up minerals found within the cavity and contained within some amorphous cement. The amorphous material appears in two distinct colors: brown and gray (Figure 2.17).

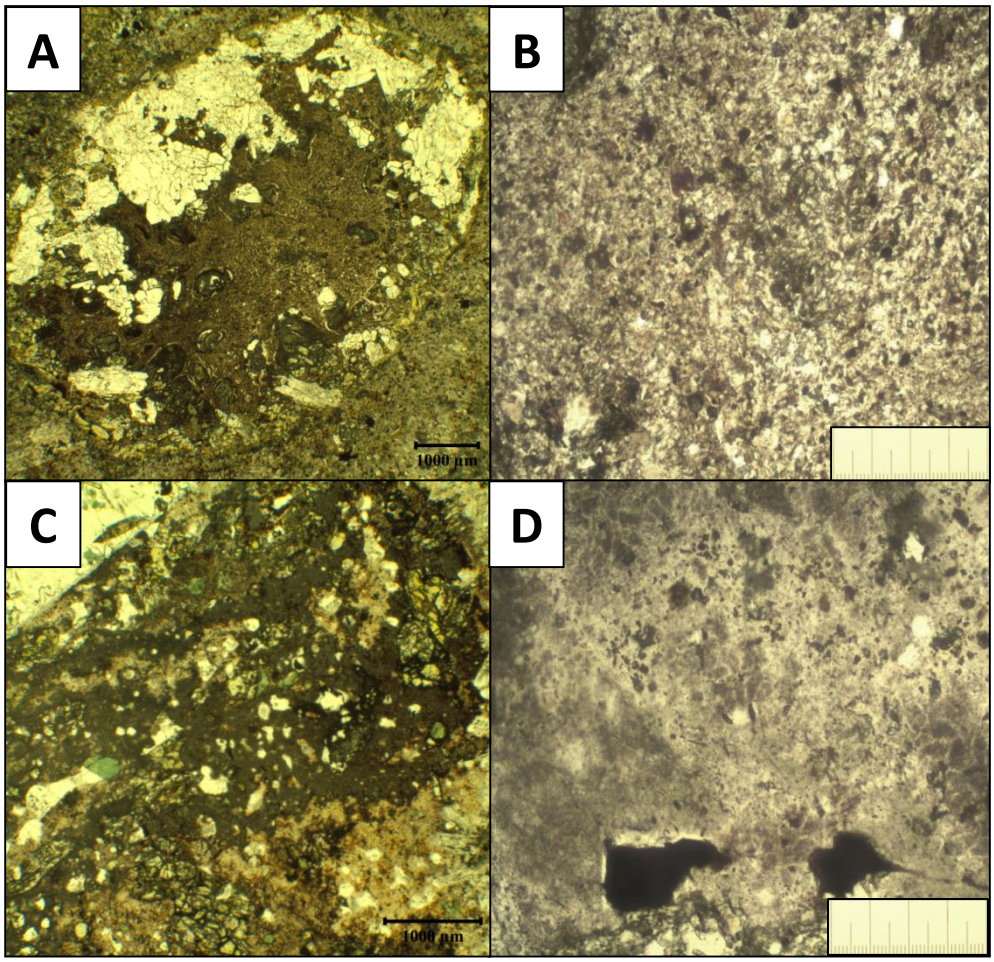

Figure 2.17. (A) Microphotograph of brown amorphous mass found in a miarolitic cavity within sample TJ-5; (B) Zoomed in image of brown amorphous mass in (A) – each tick on scale represents 1/10th mm; (C) Microphotograph of gray amorphous mass found in a miarolitic cavity within sample TJ-2D; (D) Zoomed in image of gray amorphous mass in (C) – each on scale tick represents 1/10th mm.

Chapter III
MINERAL CHEMISTRY

Introduction

Mineral chemistry in oxide weight percent for epidote (Tables 3.1 and 3.2), chlorite (Table 3.3), and muscovite (Table 3.4) were obtained using electron microprobe analysis. The focus of the mineral chemistry data was to better understand the chemical relationships implied by the zonation observed in epidotes and the variations in the color of chlorite described in the previous chapter.

Epidote

From 7 samples, 15 unzoned epidotes (Table 3.1) and 5 zoned epidotes (Table 3.2) were analyzed. Figure 3.1 displays the weight percent Fe_2O_3 versus Al_2O_3 results for all the epidotes. The results for zoned epidote, which vary in color from a light pale green in the center to a darker yellow green at the rims (Figure 2.5) indicated a negative correlation between aluminum and iron abundances. As the zoned epidote grew out from the center towards the rim, iron began becoming preferentially incorporated into the crystal lattice at the expense of alumina. This resulted in the zonation between a more aluminum-rich clinozoisite-like center to a more iron-rich epidote rim, and a darkening of the color of the rim due to the increase in iron. Unzoned epidotes in different samples span almost the full range of compositions observed in the zoned epidote crystals.

Table 3.1. Compositions of Unzoned Epidotes (Number of Ions on the Basis of 7 Cations)

Sample	**TJ-2A**	**TJ-2A**	**TJ-2A**	**TJ-3**	**TJ-3**	**TJ-3**	**TJ-4A**	**TJ-4A**	**TJ-4A**	**TJ-14**	**TJ-14**	**TJ-14**	**TJ-5**	**TJ-5**	**TJ-5**
#	**#1**	**#2**	**#3**	**#1**	**#2**	**#4**	**#1**	**#2**	**#3**	**#1**	**#2**	**#3**	**#1**	**#2**	**#3**
SiO_2	37.08	36.43	37.70	38.69	37.48	37.41	37.99	36.61	36.37	37.54	37.72	37.72	37.39	35.38	37.34
TiO_2	0.01	0.01	0.00	0.05	0.18	0.04	0.02	0.23	0.04	0.04	0.02	0.02	0.02	0.00	0.02
Al_2O_3	20.07	22.60	21.83	26.41	24.05	23.41	25.01	24.90	21.94	22.92	22.02	22.26	22.08	24.00	23.78
Fe_2O_3*	17.73	14.96	15.30	11.32	12.74	13.41	11.83	12.31	15.58	14.00	15.08	14.70	15.21	15.99	13.32
MnO	0.29	0.75	0.13	0.03	0.08	0.33	0.40	0.09	0.14	0.09	0.09	0.14	0.36	0.55	0.28
MgO	0.00	0.00	0.01	0.01	0.06	0.02	0.04	0.08	0.50	0.01	0.02	0.01	0.19	0.08	0.01
CaO	22.86	22.07	23.12	23.52	23.71	22.90	22.88	22.84	22.55	22.99	22.96	22.89	23.34	21.63	23.14
Total	**98.04**	**96.82**	**98.09**	**100.0**	**98.30**	**97.52**	**98.17**	**97.06**	**97.12**	**97.59**	**97.90**	**97.74**	**98.59**	**97.63**	**97.89**
Si	2.62	2.58	2.64	2.61	2.59	2.62	2.62	2.56	2.57	2.63	2.64	2.65	2.60	2.49	2.60
Al	1.67	1.89	1.80	2.10	1.96	1.93	2.03	2.05	1.83	1.89	1.82	1.84	1.81	1.99	1.95
Fe	0.95	0.81	0.81	0.58	0.67	0.71	0.62	0.65	0.84	0.75	0.80	0.78	0.80	0.85	0.71
Mn	0.02	0.05	0.01	0.00	0.00	0.02	0.02	0.01	0.01	0.01	0.01	0.01	0.02	0.03	0.02
Mg	0.00	0.00	0.00	0.00	0.01	0.00	0.00	0.01	0.05	0.00	0.00	0.00	0.02	0.01	0.00
Ti	0.00	0.00	0.00	0.00	0.01	0.00	0.00	0.01	0.00	0.00	0.00	0.00	0.00	0.00	0.00
Ca	1.73	1.68	1.73	1.70	1.76	1.72	1.69	1.71	1.71	1.72	1.72	1.72	1.74	1.63	1.73

*All Fe as Fe_2O_3

Table 3.2. Compositions of Zoned Epidotes (Number of Ions on the Basis of 7 Cations)

Sample #	**TJ-6 #1 center**	**TJ-6 #2 center**	**TJ-6 #2 rim**	**TJ-1 #1 center**	**TJ-1 #1 rim**	**TJ-1 #2 center**	**TJ-1 #2 rim1**	**TJ-1 #2 rim2**	**TJ-1 #3 center**	**TJ-1 #3 rim**
SiO_2	36.13	37.41	37.73	39.73	36.97	38.18	36.86	36.42	36.15	37.23
TiO_2	0.02	0.00	0.00	0.02	0.00	0.03	0.01	0.01	0.00	0.00
Al_2O_3	27.19	22.64	22.89	23.99	19.46	23.60	21.89	22.60	21.14	21.21
Fe_2O_3*	13.32	14.77	15.04	11.95	18.94	12.96	15.81	14.64	16.21	16.20
MnO	0.18	0.24	0.18	0.43	0.12	0.24	0.18	0.12	0.10	0.08
MgO	0.00	0.00	0.01	0.01	0.01	0.00	0.00	0.01	0.00	0.01
CaO	22.64	23.07	22.89	21.06	22.83	23.30	22.70	22.81	22.97	22.87
Total	**99.48**	**98.13**	**98.74**	**97.19**	**98.33**	**98.31**	**97.45**	**96.60**	**96.57**	**97.60**
Si	2.46	2.61	2.62	2.73	2.62	2.65	2.60	2.58	2.58	2.63
Al	2.18	1.86	1.87	1.95	1.62	1.93	1.82	1.89	1.78	1.76
Fe	0.69	0.78	0.79	0.63	1.02	0.68	0.85	0.79	0.88	0.87
Mn	0.01	0.01	0.01	0.03	0.01	0.01	0.01	0.01	0.01	0.00
Mg	0.00	0.00	0.00	0.00	0.00	0.00	0.00	0.00	0.00	0.00
Ti	0.00	0.00	0.00	0.00	0.00	0.00	0.00	0.00	0.00	0.00
Ca	1.65	1.73	1.70	1.55	1.73	1.73	1.72	1.73	1.76	1.73

*All Fe as Fe_2O_3

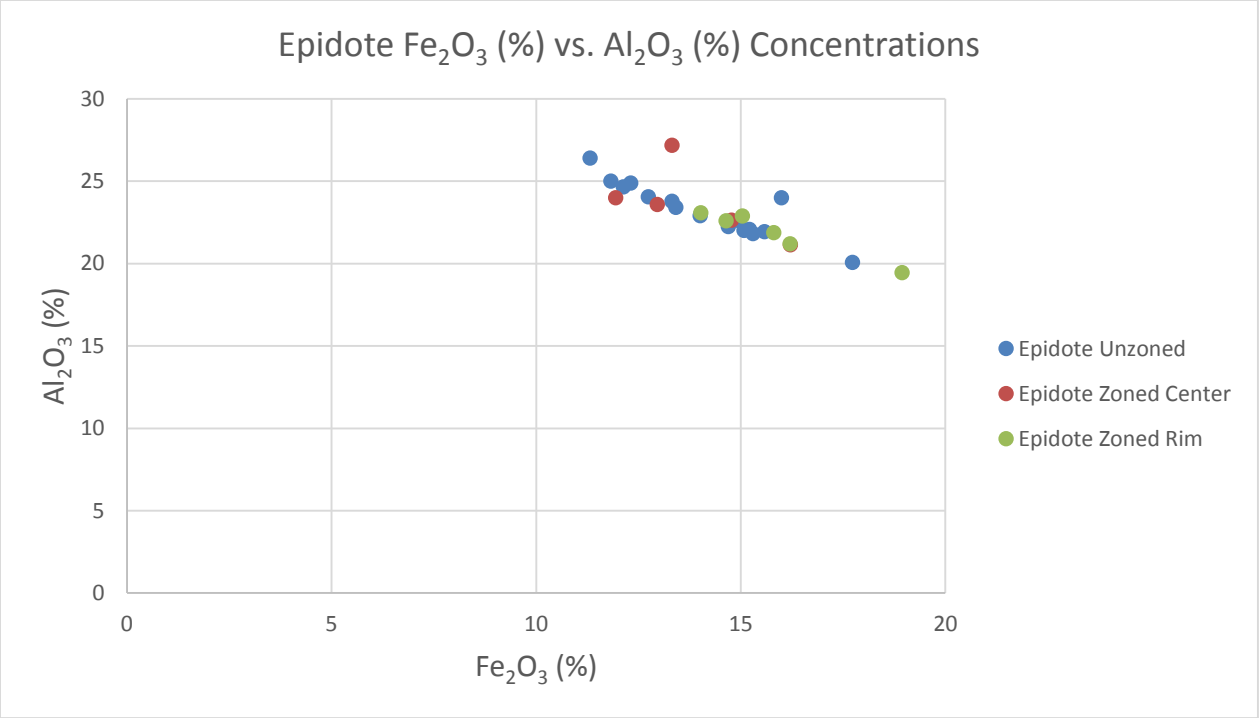

Figure 3.1. Aluminum oxide weight percentages plotted against iron oxide percentages for analyzed epidotes.

Chlorite

Chlorites from 6 samples were analyzed (Table 3.3). Note that the weight percent oxide values are low due to the lack in accounting for water. Figure 3.2 displays the weight percent Fe_2O_3 versus MgO results. Chlorites vary in color from a light pale green (Figure 2.7) to a darker green typically found at the rims (Figure 2.5) or in miarolitic cavities composed only of chlorite (Figure 2.8). The electron microprobe results for chlorite indicate an inverse correlation between magnesium and iron abundances (Figure 3.2). The darker the chlorite, the more iron is incorporated in its crystal lattice during growth.

Table 3.3. Compositions of Sampled Chlorites (Number of Ions on the Basis of 20 Cations)

	TJ-2A	TJ-2A	TJ-2A	TJ-2A	TJ-6	TJ-6	TJ-6	TJ-1	TJ-1	TJ-1	TJ-4A	TJ-14	TJ-14	TJ-14	TJ-5	TJ-5	TJ-5	TJ-5
Sample #	**#1a**	**#1b**	**#3**	**#4**	**#1**	**#2**	**#3**	**#1**	**#2**	**#3**	**#1**	**#1**	**#2**	**#3**	**#1**	**#2**	**#3**	**#4**
SiO_2	27.32	26.95	28.26	27.91	25.45	26.38	25.98	28.03	28.40	28.70	27.13	29.31	27.80	29.78	28.75	26.95	27.55	28.92
TiO_2	0.00	0.00	0.00	0.00	0.00	0.00	0.00	0.04	0.04	0.04	0.04	0.04	0.04	0.04	0.02	0.02	0.02	0.02
Al_2O_3	18.12	18.28	18.69	18.53	18.87	19.55	19.39	18.52	18.73	19.14	19.47	20.16	20.86	20.34	21.75	20.03	20.10	19.87
FeO	20.02	20.12	20.42	20.25	29.25	26.20	29.06	19.96	20.11	20.26	23.08	22.99	27.00	23.28	18.10	21.09	20.74	20.11
MnO	0.60	0.56	0.58	0.66	0.50	0.63	0.53	0.68	0.57	0.60	0.77	0.47	0.56	0.49	0.85	0.57	0.58	0.60
MgO	18.60	18.44	19.84	19.58	6.34	15.18	12.56	19.79	19.69	20.15	16.20	11.51	9.33	13.34	19.21	17.84	18.33	18.91
CaO	0.05	0.03	0.09	0.04	0.46	0.08	0.10	0.10	0.04	0.08	0.15	0.37	0.42	0.39	0.06	0.09	0.04	0.07
K_2O	0.02	0.01	0.02	0.01	0.45	0.01	0.06	0.01	0.01	0.02	0.01	0.24	0.21	0.22	0.01	0.04	0.02	0.05
Total	**84.73**	**84.39**	**87.90**	**86.98**	**84.32**	**88.03**	**87.68**	**87.13**	**87.59**	**88.99**	**86.85**	**85.09**	**86.22**	**87.88**	**88.72**	**86.63**	**87.38**	**88.54**
Si	5.83	5.78	5.79	5.79	6.12	5.58	5.62	5.79	5.84	5.80	5.75	6.47	6.17	6.32	5.81	5.65	5.71	5.90
Al	4.56	4.62	4.52	4.53	5.35	4.87	4.94	4.51	4.54	4.56	4.86	5.25	5.46	5.09	5.18	4.95	4.91	4.78
Fe	3.57	3.61	3.50	3.51	5.88	4.63	5.26	3.45	3.46	3.43	4.09	4.25	5.01	4.13	3.06	3.70	3.60	3.43
Mn	0.11	0.10	0.10	0.12	0.10	0.11	0.10	0.12	0.10	0.10	0.14	0.09	0.11	0.09	0.15	0.10	0.10	0.10
Mg	5.91	5.89	6.06	6.05	2.27	4.78	4.05	6.10	6.04	6.07	5.12	3.79	3.09	4.22	5.79	5.57	5.66	5.75
Ti	0.00	0.00	0.00	0.00	0.00	0.00	0.00	0.01	0.01	0.01	0.01	0.01	0.01	0.01	0.00	0.00	0.00	0.00
Ca	0.01	0.01	0.02	0.01	0.12	0.02	0.02	0.02	0.01	0.02	0.03	0.09	0.10	0.09	0.01	0.02	0.01	0.02
K	0.00	0.00	0.00	0.00	0.14	0.00	0.02	0.00	0.00	0.01	0.00	0.07	0.06	0.06	0.00	0.01	0.00	0.01

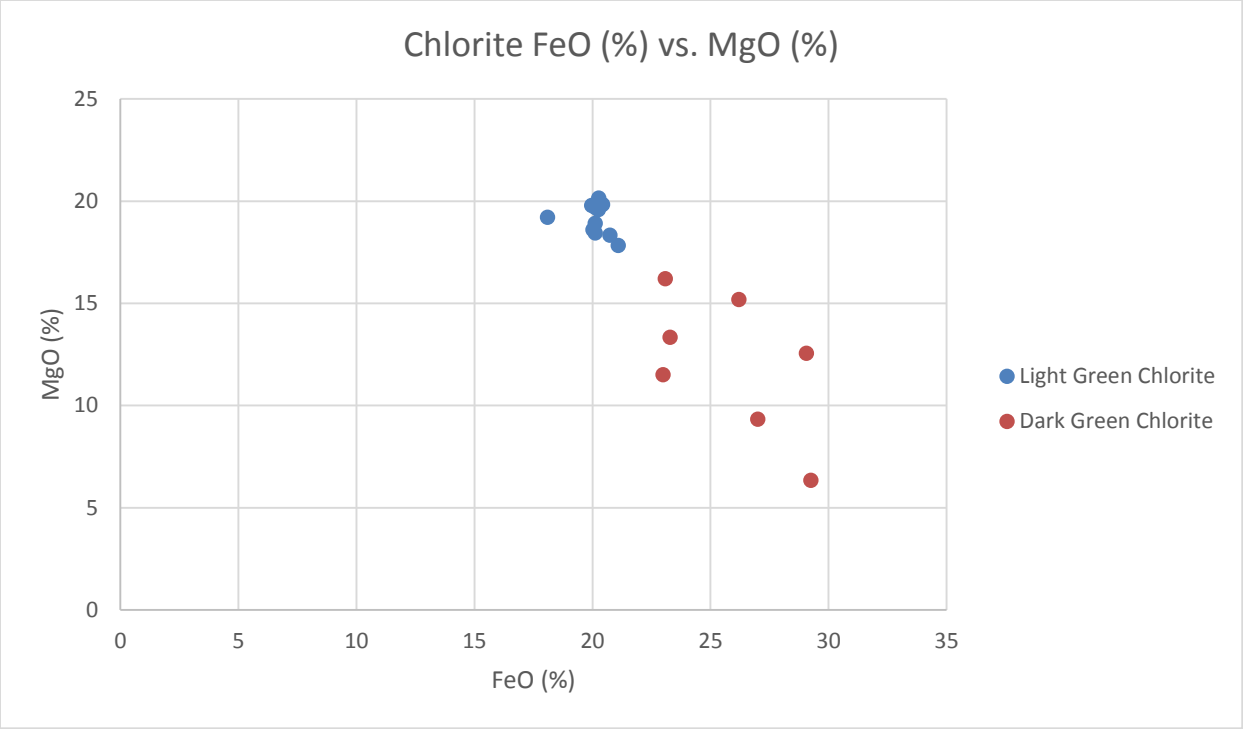

Figure 3.5. Magnesium oxide weight percentages plotted against iron oxide percentages for analyzed epidotes.

Muscovite

Two muscovite crystals from sample TJ-4A were analyzed. Table 3.4 displays the weight percent oxide and elemental abundance results on the basis of 20 cations. Note that weight percent oxide values are low due to the lack in accounting for water. The muscovites analyzed within the miarolitic cavity seem to have a significant abundance of iron incorporated in their crystal lattice.

Table 3.4. Compositions of Sampled Muscovites (Number of Ions on the Basis of 20 Cations)

Sample #	**TJ-4A**	**TJ-4A #2**
SiO_2	47.68	48.16
TiO_2	0.23	0.04
Al_2O_3	30.20	31.03
FeO	5.44	3.94
MnO	0.03	0.02
MgO	0.77	1.03
CaO	0.05	0.12
K2O	10.61	10.11
Total	**95.01**	**94.45**
Si	9.268	9.373
Al	6.92	7.118
Fe	0.884	0.6415
Mn	0.0055	0.0032
Mg	0.2234	0.2997
Ti	0.0341	0.006
Ca	0.0096	0.0251
K	2.631	2.5093

Chapter IV
PETROCHEMISTRY

Host Dikes

The miarolitic cavities are found in two altered andesitic dikes that vary in color between a light and a darker gray (Figure 4.1), and to a small degree in trace-element chemistry (Table 4.1). The dikes are both porphyritic and have a very fine grained, unaltered groundmass with many small opaques and plagioclase microlites. The darker gray dike has a little courser groundmass compared to the lighter gray dike. All the phenocrysts in both dikes have been altered to epidote and chlorite. Based on crystal shape and relict twining within the altered phenocrysts, they appear to have been amphibole and plagioclase.

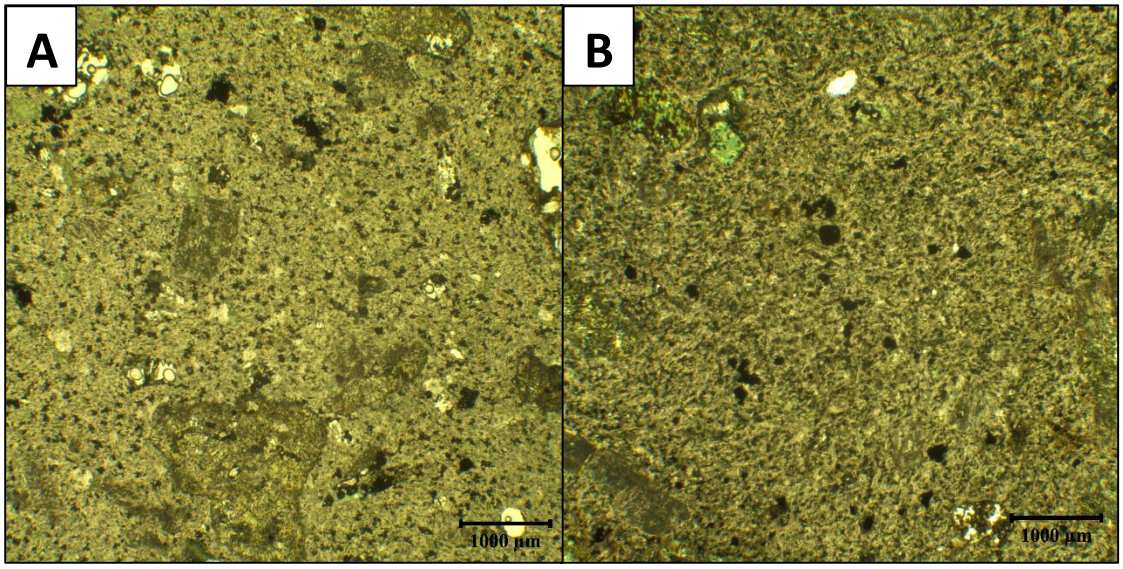

Figure 4.1. (A) Microphotograph of lighter gray host dike that has fine ground mass, several small opaques, and altered phenocrysts of plagioclase and amphibole; (B) Microphotograph of darker gray host dike that has course ground mass, several small opaques, and altered phenocrysts of plagioclase and amphibole.

Table 4.1. Host Dike Bulk Rock Chemistry (in ppm)

Sample #	Color	Ti*	V	Cr	Mn	Co	Ni	Cu	Zn	Rb	Sr	Y	Zr	Nb	Ba	Hf	Pb	Th	U
TJ-14	lighter gray	9034	221	18	1156	24	47	26	154	24	1003	22	178	56	1083	4.5	15.0	8.8	2.9
TJ-7	darker gray	8613	222	27	1204	35	52	19	148	32	872	24	154	49	1224	4.1	19.0	7.2	2.3
TJ-7 dup.	darker gray	8394	227	29	1195	36	52	18	147	33	892	23	165	50	1228	4.4	18.9	7.3	2.2

Sample #	Color	La	Ce	Pr	Nd	Sm	Eu	Gd	Tb	Dy	Ho	Er	Tm	Yb	Lu
TJ-14	lighter gray	59.6	108.6	12.2	44.2	8.1	2.6	9.2	0.99	4.59	0.77	2.38	0.27	1.79	0.21
TJ-7	darker gray	52.9	97.9	11.1	40.0	7.7	2.7	8.2	1.07	4.29	0.78	2.15	0.24	1.62	0.21
TJ-7 dup.	darker gray	54.1	98.6	10.9	38.9	7.7	2.7	8.3	1.14	4.44	0.71	2.08	0.24	1.57	0.20

Bulk trace-element chemistry was done for one sample of the lighter gray dike and one sample of the darker gray dike using ICP-MS (Table 4.1). There seems to be only a slight difference in chemistry between the two host dikes. In general, the lighter gray dike has more basalt-like chemistry than the dark dike, with higher Ti and Sr, and lower Rb and Ba, but the differences are small.

Miarolitic Cavities

Petrology

All petrologic observations for the miarolitic cavities are indicated within the following tables. These tables are organized based first on host dike (light gray or dark gray). The light gray host dike is separated further based on whether or not muscovite appeared in the samples. Since there is no observed muscovite within the miarolitic cavities from the dark gray host dike, the cavities in this dike are separated further based on the appearance or lack of calcite within the cavity. A legend to the symbols used is provided below in Table 4.2.

Table 4.2. Legend

Symbol	Meaning
Q	Quartz
Q(Z)	Quartz with Fluid Inclusion Zones
E(E)	Equant Epidote
E(F)	Fibrous Epidote
E(Z)	Zoned Epidote
Chl	Chlorite
M	Muscovite
Ca	Calcite
O	Opaque
Ba	Barite
B	Brown Amorphous Mass
G	Gray Amorphous Mass

Table 4.3 lists miarolitic cavities from the light gray host dike that do not have observable muscovite and Table 4.4 lists out the miarolitic cavities that do have observable muscovite. The rims of the cavities within the light gray host dike seem to be mostly chlorite and epidote.

Table 4.3. Light Gray Host Dike Samples with No Observable Muscovite

Sample #	Minerals Observed	Zonation		Shape	Comments and Figures
		Rim	Center		
TJ-4B	Q, E(E), Chl, O	Chl	E, Q	Circular	Mostly Chl
TJ-5	Q, E(E), E(Z), Chl, B	Chl	B, E	Circular	Fig. 2.7
TJ-6	Q, E(E), E(Z), Chl, B,G	Q, Chl	B, G	Vein	
TJ-10A	Q, E(E), Chl	Chl	Q	Circular	
TJ-10B	Q, E(E), Chl	Chl	Q	Circular	
TJ-10C	Q, E(E), Chl	Chl	Q, E	Circular	
TJ-10D	Q, E(E), Chl	Chl	E	Circular	
TJ-14	Q, E(E), B	E	B, G	Vein	Mostly E
TJ-15	Q, Q(Z), Chl, Ba	Chl	Q	Circular	
TJ-20	Q, E(E), E(F), Ba	E	Q	Vein	

Table 4.4. Light Gray Host Dike Samples with Observable Muscovite

Sample #	Minerals Observed	Zonation		Shape	Comments and Figures
		Rim	Center		
TJ-3	M, Q, Q(Z), E(E), E(F), Ca	Q	Ca, E(F)	Vein	
TJ-3B	M, Q, E(E), Ba, B, G	E	Q	Circular	
TJ-4A	M, Q, Q(Z), E(E), E(F), Chl, G	Q	E(F)	Circular	Mostly E
TJ-4C	M, Q, E(E), E(F), Chl, Ca, Ba	Chl	E	Circular	Fig. 2.9
TJ-10E	M, Q, E(E), Chl,	Chl	Q, E	Circular	
TJ-10F	M, Q, E(E), E(F), Chl, O	Chl, E	Q	Circular	Cavities connected by altered E
TJ-13A	M, Q, E(E), Chl,	Chl	Q	Circular	
TJ-13B	M, Q, E(E), E(F), Chl, B	Chl	B, G	Circular	
TJ-13C	M, Q, E(E), Ba	E	Q	Circular	Large amount of Ba
TJ-13D	M, Q, E(E), E(F), Chl,	E	Q	Circular	
TJ-13F	M, Q, E(E), Chl, B, G	E	Mix	Circular	More Micacious
TJ-16	M, Q, E(E), E(F), Ba	E	Q	Circular	

Table 4.5 lists miarolitic cavities from the dark gray host dike that do not have observable calcite and Table 4.6 lists out the miarolitic cavities that do have observable calcite. Miarolitic cavities from the darker gray host dike have more quartz rims compared to the light gray host dike.

Table 4.5. Dark Gray Host Dike Samples with No Observable Calcite

Sample #	Minerals Observed	Zonation		Shape	Comments and Figures
		Rim	Center		
TJ-1	Q, E(E), E(Z)	Q	E	Vein	Q with needle inclusions
TJ-2C	Q, E(E), Chl, O, G	Q	E, G	Circular	
TJ-2D	Q, E(E), E(F), Ba	E	Q	Vein	
TJ-7	Q, E(E), Chl, Ba, G	Ch, E	Q, G	Vein	
TJ-8B	Q, E(E), Chl, O	Varies throughout cavity		Vein	
TJ-9B	Q, E(E), E(Z), Chl	Q, Chl	E	Vein	
TJ-9C	Q, E(E), Chl	Varies throughout cavity		Circular	
TJ-9D	Q, Q(Z), E(E), Chl	Chl	Q, E	Vein	
TJ-12	Q, E(E), E(Z)	Chl	E	Vein	Q with needle inclusions
TJ-17	Q, E(E), Chl	E	E	Circular	Almost all E
TJ-18	Q, E(E), Chl, Ba	Chl	E	Vein	
TJ-19	Q, E(E), Chl	E	Q	Vein	

Table 4.6. Dark Gray Host Dike Samples with Observable Calcite

Sample #	Minerals Observed	Zonation		Shape	Comments and Figures
		Rim	Center		
TJ-2A	Q, E(E), Chl, Ca, O, Ba, G	Q	Ca, G	Circular	Fig. 2.1; Q within Ca
TJ-2B	Q, E(E), Chl, Ca, O, Ba, G	Q	G	Vein	
TJ-2E	Q, E(E), Chl, Ca, O, G	Q	Ca, G	Circular	Q within Ca
TJ-8A	Q, E(E), Chl, Ca	Chl	Q, E	Circle	
TJ-8D	Q, Q(Z), E(E), Ca, G	Q, Chl	Ca, E	Vein	
TJ-9A	Q, Q(Z), E(E), Chl, Ca	E	Q	Vein	E within Ca
TJ-11	Q, E(E), Ca, Ba	Chl	E, Ca	Vein	Abundance of Ba; E within Ca

Chemistry

Regarding the miarolitic cavity bulk trace-element chemistry (Table 4.7), the two miarolitic cavities analyzed from the light dike (TJ-3B and TJ-13E) have significantly higher barium content compared to the other three samples from the darker dike. Sample TJ-3B has barite, and although there is no thin section of TJ-13E, the thin section of TJ-13C from the same rock also has barite. This explains the high barium content within both samples.

The three samples from the darker dike have variable bulk trace element chemistry. Samples TJ-2B and TJ-2E are similar in many respects as they have similar and relatively high Cu and Co contents compared to the other sample, which is consistent with the presence of chalcopyrite and the cobalt sulfide observed in the thin section of sample TJ-2A cut from the same rock. Sample TJ-18 has the highest titanium and lead abundances and differs in these respects from TJ-2B and TJ-2E despite being derived from the same host dike.

Table 4.7. Miarolitic Cavity Bulk Rock Chemistry (in ppm)

Sample #	Host Dike Color	Ti*	V	Cr	Mn	Co	Ni	Cu	Zn	Rb	Sr	Y	Zr	Nb	Cs	Ba
TJ-2B	Darker Gray	1022	155	7	2775	54	30	1818	93	46	840	10	13	6	0.3	3640
TJ-2E	Darker Gray	657	136	5	2314	50	34	1581	70	15	919	6	9	4	0.2	3976
TJ-18	Darker Gray	2883	205	22	2308	26	35	737	710	30	1302	10	43	15	0.4	4776
TJ-3B	Lighter Gray	336	240	6	2070	14	30	75	46	18	1875	5	3	1	DL	52052
TJ-13E	Lighter Gray	494	112	3	1116	14	18	41	61	57	1346	4	7	2	0.4	>50000

Sample #	Host Dike Color	La	Ce	Pr	Nd	Sm	Eu	Gd	Tb	Dy	Ho	Er	Tm	Yb	Lu	Hf	Pb	Th	U
TJ-2B	Darker Gray	34.9	28.8	5.8	21.3	7.0	4.1	4.3	0.5	1.8	0.3	0.8	0.1	0.4	DL	0.6	26.4	1.6	0.7
TJ-2E	Darker Gray	15.1	20.1	2.6	9.3	5.6	3.6	2.5	0.3	1.1	0.2	0.5	DL	0.3	DL	0.2	110.3	0.9	0.4
TJ-18	Darker Gray	33.6	57.4	6.4	22.0	7.9	4.3	5.0	0.4	2.0	0.3	1.0	0.1	0.8	DL	1.3	617.0	3.0	1.2
TJ-3B	Lighter Gray	19.6	18.6	1.3	4.3	49.4	35.3	1.2	0.1	0.4	DL	0.3	DL	0.2	DL	0.2	81.4	0.7	0.5
TJ-13E	Lighter Gray	8.4	16.1	1.1	4.4	52.4	35.4	1.0	0.1	0.5	DL	0.2	DL	DL	DL	0.3	13.5	0.8	0.3

Chapter V
DISCUSSION AND CONCLUSION

Mineralogy and Chemistry of the Cavities

Throughout all the miarolitic cavities that were observed under the microscope and analyzed with the electron microprobe and ICP-MS, there is an abundance of chlorite and epidote. This observation, in conjunction with the absence of any feldspar in any of the miarolitic cavities examined, suggests that these miarolitic cavities are somewhat different from those observed in association with granites. Based on the mineralogy and elemental chemistry data (Chapter II and IV), Si, Al, Fe, Mg, Ca, S, Cu, Ba, and Co were clearly mobilized within both dikes. However, potassium was mobilized only in the light gray host dike, but not in the dark gray host dike as there was no muscovite or other potassium bearing minerals found in the miarolitic cavities of the dark gray host dike. Also, no sodium bearing phase was observed in any of the miarolitic cavities.

The mobilization of the elements within the fluid that mineralized the cavities is indicated by the minerals present within these cavities: Silica is indicated by the presence of quartz and other silicate minerals; Aluminum by epidote, chlorite, and muscovite; Iron by epidote, chlorite, hematite; Magnesium by chlorite and epidote; Calcium by epidote and calcite; Potassium by muscovite; Sulfur by pyrite, chalcopyrite, barite, and the cobalt sulfide; Copper by Chalcopyrite; Barium by barite; and Cobalt by the cobalt sulfide. The fluids that deposited these minerals must have been a mixture of H_2O, CO_2 and SO_2.

It is noteworthy that there is a complete absence of sodium within the cavities since it is normally a mobile element. This suggests that sodium mobilization may have been inhibited by another process. It can be speculated that sodium may have been caught up within the plagioclase of the host dike, changing Ca-plagioclase into Na-rich plagioclase without modifying

the texture of the rock such as occurs during “spilitization” of ocean floor basalts. Spilitization is essentially greenschist facies metamorphism of igneous rocks by heated (>200°C) seawater during which Na gets trapped in the plagioclase and Ca gets mobilized into the hot fluids. Unfortunately, the plagioclase in the host rock was not probed to determine its composition to test this suggestion.

Depth and Conditions of Formation

All samples were collected from scree found approximately 540 m below the peak of West Spanish Peak. Taking into account the consideration that another 500 m of Tertiary sediments, if not more, have probably been removed from above this peak by erosion, as indicated by the fact that the WSP granite contains orthoclase and is holocrystalline, the miarolitic cavities found would have been formed approximately >1000 m below the paleosurface. This depth, in combination with the observed greenschist facies minerals (chlorite and epidote) in the cavities suggests a formation temperature of 200 – 400°C. There appears to have been no low temperature alteration within either host dikes.

Origin of Fluids

The presence of miarolitic cavities within both host dikes suggests that fluids were exsolved from the dike-forming magma and then expanded to form the cavities. Then these fluids flowed throughout both of the dikes, altering them and finally depositing minerals into the cavities. Both dikes went through this deuteric alteration in which the fluids and elements that altered each dike came from the magma itself. This means that both dikes must have had H_2O, CO_2, and SO_2 present within the magma to begin with as is indicated by the minerals present within the cavities.

Implications

The processes of alteration and miarolitic cavity formation by magmatic fluids at high T have many similarities with the processes involved in the formation of ore deposits. The presence of Cu and Co sulfides in the miarolitic cavities indicates that metals were mobilized by the fluids that formed the cavities and that the Spanish Peaks area might be a region of potential economic ore deposits. Such deposits are found associated with similar age tertiary intrusions south of Spanish Peaks, such as the Questa Mo deposit in northern New Mexico.

Future Work

All samples used for this study were collected from the site indicated on Figure 1.3. However, the host dikes appear to go up further to the peak of West Spanish Peak. Further work examining the vertical continuity of the host dikes along with cavity size and mineral changes as height increases may give a better understanding of how the fluids evolved as they rose towards the surface.

Although fluid inclusions within quartz found in the miarolitic cavities were observed, this study was too limited in time and resources and therefore unable to analyze them. Analyzing these fluid inclusions may result in a better understanding of the volatiles present during mineralization within the cavity and at what depth and temperature conditions these minerals where precipitated.

Another interesting possibility for future work includes microprobing the host dikes to better understand where the potassium and sodium went. It is speculated that the sodium replaced calcium in plagioclase during alteration. However, microprobing the host dikes may give better insight of the alteration processes that occurred inside the dike.

Strontium isotopic data from the minerals both in the cavities and their respective host dikes could also confirm that deuteric alteration is the source for the elements that occur in the miarolitic cavities. If the isotopic ratio of Sr^{87} to Sr^{86} is similar within the minerals in the cavities to that of the host dike, it is then consistent with the fluid that precipitated the minerals having been derived from the host rock. If these isotopic ratios are different then the fluid would have had to come from somewhere else.

Closer investigation of the miarolitic cavities found within these two altered andesitic dikes could potentially lead to the discovery of a fruitful ore deposit. The finding of just one small grain of a rare cobalt sulfide (either cattierite or linnaeite) by chance, means that there must be more within the immediate region. Therefore, further study of the miarolitic cavities found in West Spanish Peak, CO may be worth the potential economic value.

Acknowledgements

I would like to thank Charles Stern who introduced me to this project and spent countless hours guiding me through the correct processes and thesis revisions, Alexandra Skewes for her advice and knowledge about miarolitic cavities, Julian Allaz for instruction and assistance in the use of the electron microprobe, Fred Luiszer for the ICP-MS rare earth element chemical analysis, Markus Raschke and Rebecca Flowers for their time and advice with thesis drafting, and especially Paul Boni for the hours spent walking me through the thin section making processes and continuously supporting me along the way. I would also like to thank Lang Farmer and the department of Geological Sciences, as well as the Undergraduate Research Opportunities Program (UROP) for funding this honors thesis project.

REFERENCES

Candela, P. A., and Blevin, P. L., 1995, So Some Miarolitic Granites Preserve Evidence of Magmatic Volatile Phase Permeability?: Economic Geology, v. 90, p. 2310-2316.

Frezzotti, M. L., 1992, Magmatic immiscibility and fluid phase evolution in the Mount Genis granite (southeastern Sardinia, Italy): Geochimica et Cosmochimica Acta, v. 56, p. 21 - 33.

Hutchinson, R. M., and Vine, J. D., 1987, Alteration zones related to igneous activity, Spanish Peaks area, Las Animas and Huerfano counties, Colorado: Geological Society of America Centennial Field Guide– Rocky Mountain Section, v.2, p.357 - 360.

Johnson, R. B., 1961, Patterns and Origin of Radial Dike Swarms Associated with West Spanish Peak and Dike Mountain, South-Central Colorado: Geological Society of America Bulletin, v. 72, p. 579 - 590.

Kamenetsky, V. S., Achterbergh, E., Ryan, C. G., Naumov, V. B., Mernagh, T. P., and Davidson, P., 2002, Extreme chemical heterogeneity of granite-derived hydrothermal fluids: An example from inclusions in a single crystal of miarolitic quartz: Geology, v. 30, no. 5, p. 459 - 462.

Kile, D. E., and Eberl, D. D., 1999, Crystal growth mechanisms in miarolitic cavities in the Lake George ring complex and vicinity, Colorado: American Mineralogist, v. 84, p. 718 - 724.

Kurosawa, M., Ishii, S., and Sasa, K., 2010, Trace-element compositions of single fluid inclusions in the Kofu granite, Japan: Implications for compositions of granite-derived fluids: Island Arc, v. 19, p.40 - 59.

London, D., Morgan VI, G. B., Paul, K. A., and Guttery, B. M., 2012, Internal evolution of miarolitic granitic pegmatites at the Little Tree Mine, Ramona, California, USA: The Canadian Mineralogist, v. 50, p. 1025 – 1054.

Miggins, D. P., 2002, Chronologic, Geochemical, and Isotopic Framework of Igneous Rocks within the Raton Basin and Adjacent Rio Grande Rift, South-Central Colorado and Northern New Mexico, [Master Thesis]: Boulder, University of Colorado at Boulder, 417p.

Muller, O. H., 1986, Changing stresses during emplacement of the radial dike swarm at Spanish Peaks, Colorado: GEOLOGY, v. 14, p. 157 - 159.

Penn, B. S., and Lindsey, D. A., 2009, $^{40}Ar/^{39}Ar$ dates for the Spanish Peaks intrusions in south-central Colorado: Rocky Mountain Geology, v. 44, no.1, p. 17 - 32.

Peretyazhko, I. S., 2010, Genesis of Mineralized Cavities (Miaroles) in Granitic Pegmatites and Granites: Petrology, v. 18, no. 2, p. 183 - 208.

Pezzotta, F., Hawthorn, F. C., Cooper, M. A., and Teertstra, D. K., 1996, Fibrous Foitite from San Piero in Campo, Elba, Italy: The Canadian Mineralogist, v. 34, p. 741 - 744.

Pollard, P. J., Andrew, A. S., and Taylor, R. G., Fluid Inclusion and Stable Isotope Evidence for Interaction between Granites and Magmatic Hydrothermal Fluids during Formation of Disseminated and Pipe-Style Mineralization at the Zaaiplaats Tin Mine: Economic Geology, v. 86, p. 121 – 141.

Smith, R. P., 1975, Structure and petrology of Spanish Peaks dikes, south central Colorado, [Ph.D. dissert.]: Boulder, University of Colorado at Boulder, 191p.

Stormer, J. C., 1972, Ages and Nature of Volcanic Activity on the Southern High Plains, New Mexico and Colorado: Geological Society of America Bulletin, v. 83, p. 2443 - 2448.